

## Accepted Manuscript

Origin of the Kaviro lead deposit in the Neyganan area, Lut Block, Eastern Iran: Constraints from geology, fluid inclusions, and isotope geochemistry

Zahra Karimi Saeidabadi, Mohammad Hassan Karimpour, Azadeh Malekzadeh Shafaroudi, Behnam Rahimi, Fernando Corfu



PII: S0375-6742(17)30608-8  
DOI: doi:[10.1016/j.gexplo.2018.06.006](https://doi.org/10.1016/j.gexplo.2018.06.006)  
Reference: GEXPLO 6153

To appear in: *Journal of Geochemical Exploration*

Received date: 28 August 2017  
Revised date: 2 June 2018  
Accepted date: 8 June 2018

Please cite this article as: Zahra Karimi Saeidabadi, Mohammad Hassan Karimpour, Azadeh Malekzadeh Shafaroudi, Behnam Rahimi, Fernando Corfu , Origin of the Kaviro lead deposit in the Neyganan area, Lut Block, Eastern Iran: Constraints from geology, fluid inclusions, and isotope geochemistry. *Gexplo* (2018), doi:[10.1016/j.gexplo.2018.06.006](https://doi.org/10.1016/j.gexplo.2018.06.006)

This is a PDF file of an unedited manuscript that has been accepted for publication. As a service to our customers we are providing this early version of the manuscript. The manuscript will undergo copyediting, typesetting, and review of the resulting proof before it is published in its final form. Please note that during the production process errors may be discovered which could affect the content, and all legal disclaimers that apply to the journal pertain.

Origin of the Kaviro Lead Deposit in the Neyganan area, Lut Block,  
Eastern Iran: Constraints from Geology, Fluid inclusions, and Isotope  
geochemistry

Zahra Karimi Saeidabadi: Research Center for Ore Deposits of Eastern Iran, Faculty of Science,  
Ferdowsi University of Mashhad, P.O.

Box No. 91775-1436, Mashhad, Iran.

Email: Za\_ka120@stu.um.ac.ir

\*Mohammad Hassan Karimpour: Research Center for Ore Deposits of Eastern Iran, Faculty of  
Science, Ferdowsi University of

Mashhad, P.O. Box No. 91775-1436, Mashhad, Iran. Tel/fax: +98 513 8797275.

Email: karimpur@um.ac.ir

Azadeh Malekzadeh Shafaroudi: Research Center for Ore Deposits of Eastern Iran, Faculty of  
Science, Ferdowsi University of

Mashhad, P.O. Box No. 91775-1436, Mashhad, Iran.

Email: Shafaroudi@um.ac.ir

Behnam Rahimi: Research Center for Ore Deposits of Eastern Iran, Faculty of Science, Ferdowsi  
University of Mashhad, P.O. Box No. 91775-1436, Mashhad, Iran.

Email: b-rahimi@ferdowsi.um.ac.ir

Fernando Corfu: Section of Geology and Geophysics, Department of Geosciences, University of  
Oslo, Blindern, N-0316 Oslo, Norway.

Email: fernando.corfu@geo.uio.no

## Abstract

The Kaviro lead deposit is located in the Lut Block, which is an important metallogenic province in Eastern Iran (lat 34°22'N, long 57°18'E). The deposit includes ore-bearing veins and veinlets emplaced in folds and hosted by middle Jurassic slate units. The ore-forming procedure can be segregated into three stages: pre-mineralization stage quartz-pyrite, main stage quartz-dolomite-pyrite-galena, and late stage calcite and pyrite. Hydrothermal alteration minerals are composed of dolomite, quartz, and calcite. Microscopic surveys show that the vein includes galena with minor amounts of pyrite as hypogene minerals. Two types of fluid inclusions are distinguished in quartz and dolomite veins. Microthermometric investigations reveal homogenization temperatures of 180-250 °C and salinities from 5 to 12.5 wt.% NaCl equivalents. The ore-forming fluids of the Kaviro deposit are medium-to-low in terms of temperature and salinity. The  $\delta^{34}\text{S}$  values for the ore fluid are estimated to be between +0.94‰ and +3.27‰. The isotopic compositions of sulfur suggest that the ore-forming aqueous solutions are derived from a nonmagmatic source, probably from leaching of metamorphic rocks. The  $^{206}\text{Pb}/^{204}\text{Pb}$ ,  $^{207}\text{Pb}/^{204}\text{Pb}$ , and  $^{208}\text{Pb}/^{204}\text{Pb}$  ratios of the samples span narrow ranges from 18.514-18.569, 15.668-15.715, and 38.803-38.950, respectively. The  $^{207}\text{Pb}/^{204}\text{Pb}$  and  $^{208}\text{Pb}/^{204}\text{Pb}$  ratios plot above the evolution curves and clearly indicate a crustal source. The  $^{207}\text{Pb}/^{204}\text{Pb}$  vs.  $^{206}\text{Pb}/^{204}\text{Pb}$  data suggest a homogen source for Pb. Most of the galena samples in the CIM Pb-Zn deposits show high  $^{207}\text{Pb}/^{204}\text{Pb}$  ratios, indicating that Pb is mainly derived from continental crust or pelagic sediment. The age of the mineralization is after the middle Jurassic. The Kaviro deposit is a metamorphic-related vein deposit, and fluid mixing is the important mechanism for its deposition.

**Keywords:** Galena; Ore-forming fluid; Pb isotope; Lut Block.

## 1. Introduction

Extensive parts of Iran consist of micro-continental plates derived from Gondwana and are restricted by ophiolitic suture zones, which show the opening and closing of Paleotethyan (during the Mesozoic, Main-Cimmerian orogenesis) and Neotethyan (during the Cenozoic, Laramide orogenesis) ocean basins (Stöcklin, 1968, 1974; Berberian and King, 1981; Sengör, 1990; Stampfli and Borel 2002; Golonka, 2004; Robertson, 2007; Bagheri and Stampfli, 2008). Among this package, the Central Iranian Microcontinent (CIM; Takin, 1972) shows a territorial vast terrane in the eastern part of the country (Fig. 1a), which itself is a piece of the larger Central Iran Province. All margins of the CIM are bordered by ophiolitic residues of Neotethyan oceans that were developed at different times such as between the Upper Permian/Lower Triassic to Cretaceous during rifting, sea-floor spreading and NNE-directed drift of the CIM from the Arabian plate (Berberian and King, 1981; Alavi, 1994; Mohajjel et al., 2003; Ramezani and Tucker, 2003; Agard et al., 2006). The CIM consists of at least three main crustal parts, which are the Yazd, Tabas and Lut Blocks (Fig. 1a; Takin, 1972; Berberian and Berberian 1981). These blocks are isolated by deep-reaching fault zones (largely dextral strike-slip faults), with powerful earthquakes acting in historic times that document the current deformation related to the Arabia-Eurasia collision (Berberian and Yeats, 1999; Walker and Jackson, 2004; Walker et al., 2009).

The Lut Block, in eastern CIM, is restricted to the east by the Nehbandan Fault and Sistan Suture Zone, to the west by the Nayband Fault, and to the north by the Doruneh and related faults (the Sabzevar Zone). The Makran Arc, consisting of the Bazman Volcanic Complex and the Jaz-Murian Depression, delineates the southern border of the Lut Block (Karimpour et al., 2011) (Fig. 1a). The Lut Block has a composite tectonic evolution and is distinguished by vast magmatic activity and intensive geochemical signatures. This block is the principle metallogenic domain in eastern Iran (Karimpour et al., 2012) that entails many porphyry Cu and Cu–Au deposits, such as the Gazu deposit (Mahdavi et al., 2016), Maher-Abad, Khopik (Malekzadeh Shafaroudi et al., 2012, 2015), and Dehsalm (Arjmandzadeh and Santos 2014), Au-Ag epithermal deposits (e.g., Sheikh Abad and Hired; Richard et al., 2012), iron oxide deposits (IOCG, e.g., Qaleh-Zari; Karimpour, 2005), and Cu–Pb–Zn vein-type deposits (e.g., Khur, Sechangi; Malekzadeh Shafaroudi and Karimpour, 2013a, 2015) (Fig. 1b).

According to Ghazanfari (1993), there are four important metallogenic provinces (with considering the number of Pb-Zn deposits) in Iran, which are the Sanandaj–Sirjan zone (SSZ), Urumieh–Dokhtar zone (UDZ), Central Iran Microcontinent (CIM), and Alborz zone (AZ). New surveys have been implemented on the Pb isotopic compositions of Pb-Zn deposits in Iran, including those of the Anguran Zn-Pb deposit (Gilg et al., 2006), Emarat Zn-Pb deposit (Ehya et al., 2010), Chahgaz Zn-Pb deposit (Mousivand et al., 2011), and Shahmirzad Zn-Pb deposit (Bazargani-Guilani et al., 2011). Lancelot et al. (1997) denoted Pb isotope ratios of galena from five Iranian Pb-Zn deposits, and Mirnejad et al. (2011) reported Pb isotopic compositions of 18 Zn-Pb deposits and their occurrences within the Sanandaj-Sirjan Metamorphic Zone, Urumieh-Dokhtar Volcanic Belt, and one deposit in the Zagros Fold-Thrust Belt. Mirnejad et al. (2015) also presented Pb isotopic compositions for 14 Pb-Zn deposits within the tectonic zones of Alborz and Central Iran. Information on the genesis and age of Zn–Pb ore deposits in Iran, particularly that available to international readers, is scarce. Even though many of these deposits are considered MVT (Mississippi-Valley-Type; Ghorbani, 2002), there are important arguments about the accurate timing of mineralization and the source of the metals. Many of the Zn–Pb deposits in Iran have traditionally been considered to have formed during the Precambrian or Paleozoic (e.g., Samani, 1988) based simply on their spatial association with older country rocks. However, recent radiometric dating has yielded much younger ages (Gilg et al., 2006).

Various models/hypotheses have been recommended to clarify how some of the Zn-Pb deposits in Iran have been formed. These are composed of 1- syngenetic and epigenetic sources (Ziserman and Momenzadeh 1972; Karimzadeh, 1992; Vanaei, 1998); 2- MVT-type deposits (Forster, 1978; Ehya et al., 2010); 3- hydrothermal solutions coming from intruded batholith at depth (Rahimpour-Bonab, 1991); 4- formation by deposition of low-grade metal-bearing sediments with subsequent remobilization and concentration of the metals as economic accumulations (Momenzadeh and Rastad, 1973); 5- submarine exhalative sources for the metals that were subsequently deposited in near-shore shallow waters in the occurrence of organic materials (Momenzadeh, 1976); and 6- by mobilization of metals in host rocks with subsequent reconcentration into veins (Shojaat, 1992).

The Neyghanan region includes different mineralizations composed of occurrences of iron, copper, antimony, gold, and lead (Fig. 2). The Kaviro deposit is the most important abandoned mine in the Neyghanan region. The deposit is a vein-veinlet deposit in the Lut Block mineral

district. The mining history of the Kaviro deposit goes back to ancient times. Many vertical shafts still exist in the area but are inaccessible due to the collapse and infilling of the walls. To date, no detailed surveys on mineral paragenesis, fluid evolution and ore genesis have been fulfilled. Therefore, the studies described here are focused on geological investigations that include field geology, ore microscopy, fluid inclusion microthermometry of coexisting transparent gangue minerals (such as quartz and dolomite), the sulfur isotopic composition of galena samples, and Pb isotopes of galena, which led to a genetic model of the Kaviro lead deposit.

## 2. Geological setting

### 2.1. Regional geology

The Kaviro deposit is located in the northwest corner of the Lut Block, entailing the Neyganan region (Fig. 1b). This deposit is located in the northwestern South Khorasan Province, Iran, approximately 10 km northwest of the Neyganan region and 55 km northwest of Boshrouyeh (lat  $34^{\circ}22'N$ , long  $57^{\circ}18'E$ ) (Figs. 1b and 2).

Because there are some similarities in the sedimentary records of the Paleozoic between the Central Iran micro-continent and Arabian platform, it is believed that the CIM paleogeographic position was close to the northern border of Gondwanaland (Zarrinkoub et al., 2012). Davoudzadeh and Schmidt (1984) posited that severe orogenic movements during the Mesozoic and Tertiary triggered the breaking and splitting of this platform, which gave rise to local activations of various lineaments that isolated Central Iran into different micro-continental blocks (Yazd, Tabas, and Lut) after collision with the Turan plate. Many micro-continental and island-arc pieces are consolidated between multiple suture zones that appear on the Sistan Suture Zone (Richards et al., 2012). The aspects of Late Cretaceous ophiolites and ophiolitic mélanges appearing on the Sistan Suture Zone (mentioned also as the Sistan Ocean, which separated the Lut and Afghan Blocks), including the Birjand and Nehbandan ophiolitic complexes (Fig. 1), are summarized in Ghazi et al. (2004) and Moghadam et al. (2010).

The Lut Block is a long inflexible bulk trending north-south and is approximately 900 km in length and approximately 200 km in width (Stöcklin and Nabavi, 1973; Karimpour and Stern, 2009). Sedimentary strata in the Lut Block were principally deposited before the Permian and contain shallow marine carbonates, shales and sandstones (Stöcklin et al., 1971). Continental

Neogene sedimentary deposits and Quaternary sand dunes, salt flats and alluvial fans have spread over vast areas of the Lut Block. Although many surveys on tectonic and magmatic evolution of the Lut Block have been conducted to date, the paleotectonic of the Lut Block is extremely controversial. Some researchers (Tarkian et al., 1982; Jung et al., 1983; Samani and Ashtari, 1992) have considered the Lut Block to be within an extensional environment. Saccani et al. (2010) argued for an eastward intra-oceanic subduction due to the occurrence of ophiolitic complexes in Eastern Iran between the Lut and Afghan Blocks. Recently, asymmetric subduction models have become a subject of arguments regarding a situation similar to that of the Lut Block (Doglioni et al., 2009; Arjmandzadeh, 2011; Arjmandzadeh et al., 2011). The prolonged exposure of Tertiary volcanic and subvolcanic rocks is a particular feature of the Lut Block. These rocks enclose half of the Lut block with a thickness of 2000 m and have become organized due to subduction prior to the collision of the Arabian and Asia Plates (Camp and Griffis, 1982; Tirrul et al., 1983; Berberian et al., 1999).

The Lut Block was influenced by severe magmatism. Most of the unprotected rocks within the Lut Block are volcanic and plutonic rocks (Karimpour et al., 2011) (Fig. 1b). Outcrops of igneous rocks enclose an area of approximately 300 km × 400 km, which is a minimum calculation because their exposure might reach far into western Afghanistan (Richards et al., 2012). Quaternary desert sands spread over a vast area of the Lut Block, spatially to the south in the Dasht-e-Lut desert, which shows the Lut Depression (Mahmoudi et al., 2010). The magmatic activity in the Lut Block was established in the middle Jurassic from 165-162 Ma and reached its maximum in the Tertiary (Karimpour et al., 2011). Further to the north, magmatic activity began in the Upper Cretaceous and produced both volcanic and intrusive rocks (Tarkian et al., 1982). The Middle Eocene is distinguished via alkaline and shoshonitic volcanism, which reached its maximum at the end of the Eocene. Eocene-Oligocene magmatism in eastern Iran is reflected by extended volcanic lavas and pyroclastic rocks, subvolcanic rocks, and small separated plutons (Pang et al., 2013). The Kaviro deposit is situated in the northwest of the Lut Block. Most of the base metal vein deposits in the Lut Block are hosted within igneous rocks (Fig. 1b). Fault and folds are well-developed in the Kaviro deposit. The faults are principally NW- and NE-trending (Routner et al., 1994).

Nayband fault: The 290-km-long Nayband strike-slip fault is the western margin of the Lut Block that drifted northward from Gondwana in the framework of multiple Tethys evolutions (e.g., Berberian and King, 1981; Besse et al., 1998; Zanchi et al., 2009 and recent review by Agard et al., 2011 with references therein). At the regional scale, the Nayband fault is located between two domains of contrasting topography: the relatively high Tabas Block to the west in Central Iran and the low subducted depression of the Lut Block to the east in Eastern Iran.

Kalmard fault: This fault is a deep and ancient fault of the Central Iranian Microcontinent that formed due to the Katangaei event. Like the other faults of central Iran of Precambrian age, its initial trend is north-south. This fault is curved toward the west such that its northern part in the Shirgesht area has a north-north east trend and its south part has a southwest trend. In the Shirgesht area, the sediments of Permian and Triassic are not the same on both sides of the fault. In the west of the fault, the Permian-Triassic sediments are deformed and have low thickness, but the sediments in the east of the fault have a greater thicknesses (Routner et al., 1994). In the Kalmard area, the fault dip is 75 to 80 to the west, and it seems that the western block deviates to the east.



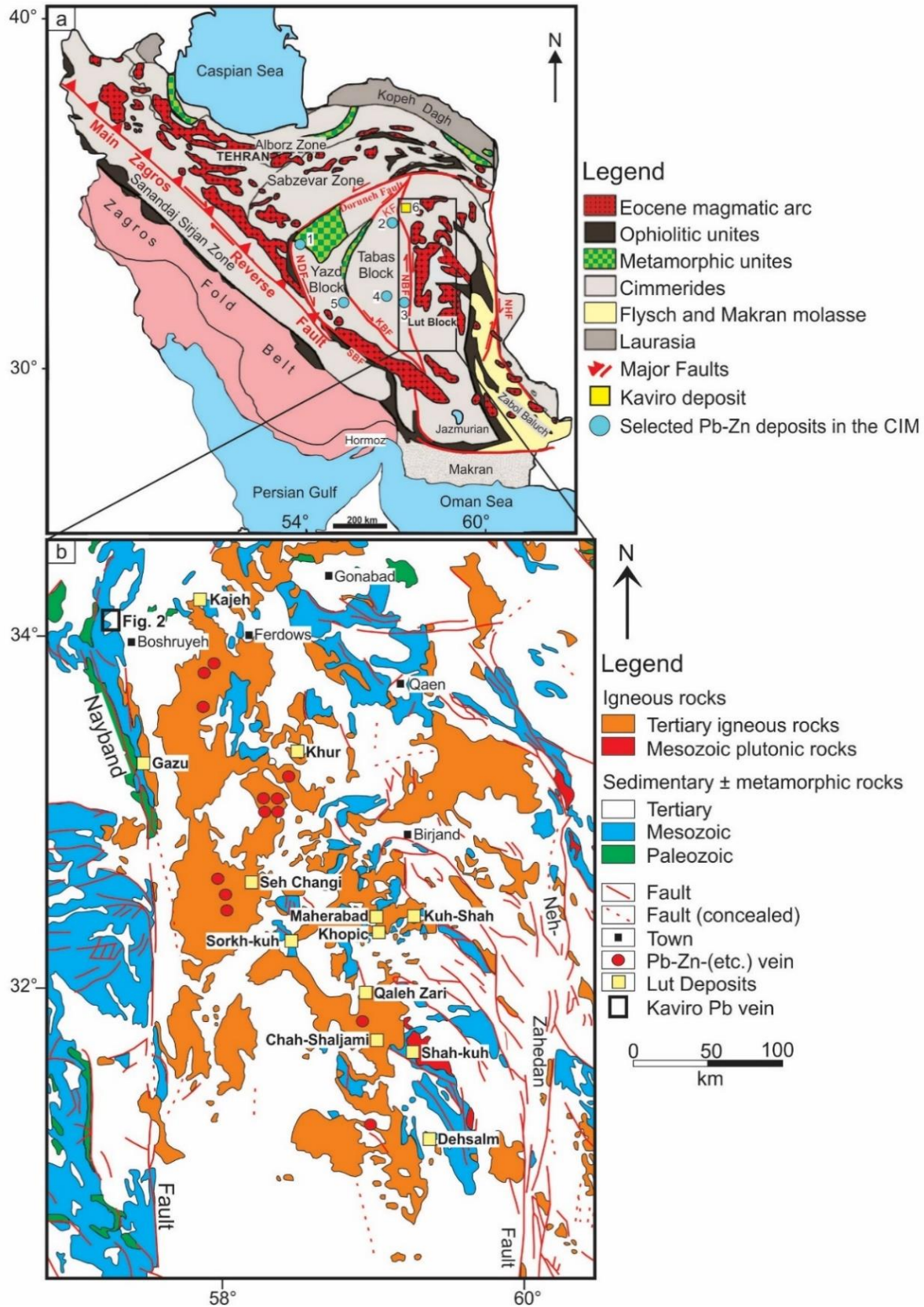


Figure 1. (a) structural map of eastern and central portions of Iran. The main strike–slip faults bounding the main blocks that make up Central East Iran are also indicated (modified after Stöcklin, 1968; Berberian, 1976, 1977; Berberian and King, 1981; Sengor, 1990; Hessami et al., 2003; Bagheri and Stampfli, 2008). The Yellow rectangle indicates the study area. Pb-Zn deposit abbreviations and numbers corresponding to the CIM deposits are listed in Table 4. KF: Kalmard Fault; KBF: Kuhbanan Fault; NBF: Nayband Fault; NHF: Nehbandan Fault; NDF: Nain-Dehshir Fault; SBF: Shahr-e-Babak Fault. (b) Mesozoic sedimentary rocks of the Lut block, Eastern Iran, showing the locations of Kaviro and some base metal vein-type deposits and also some important deposits in the Lut Block. Location of figure 2 is shown in the figure 1b with black rectangle. Based on the maps from the Geological Survey of Iran (1989, 2009, and different 1:250,000-series maps).

## 2.2. Local geology and structure

The Kaviro deposit located in Neyganan area is within the 1:250,000 Tabas (Stöcklin and Nabavi, 1969) and 1:100,000 Eshghabad (Routner et al., 1994) geological maps (lat 34°22'N, long 57°18'E). Jurassic units with broad extension have covered a large part of the Neyganan area (Fig. 2). The oldest unit, which is exposed at the middle part of the Neyganan area, is the thick layers of the metamorphosed Shemshak Formation trending NE-SW. The Baghamshah Formation, which consists of marly slate with thin layers of gypsum, has covered a large part of the Neyganan area (Fig. 2). The Baghamshah Formation, which has a middle Jurassic age, was named by Stöcklin and Nabavi (1969). The upper part of this formation is composed of a thick-layered lime that is known as Eshelon Lime. The formation is comparable with the Delichay Formation in the Alborz region and the Chamanbid Formation in the Kopehdagh region. The thickness of the Baghamshah Formation in Baghamshah (north of Shotori Mountains) is 495 meters, and ammonite is a common fossil in this formation (Aghanabati, 2004). This formation in the study area was affected by low-grade regional metamorphism. This unit is the host of Pb and Sb mineralization. The slate unit is seen as a strongly crushed unit and shows a semi flat topography. The Baghamshah Formation is directly located under the recrystallized limestone (with low grade regional metamorphism) of the Qaleh Dokhtar Formation. The Qaleh Dokhtar Formation is a late Jurassic, 974 meter succession of sandstone, shale, and lime (Aghanabati, 2004) (Fig. 2). Neogene sediments are seen as a set of conglomerate, red layers of gypsum, salt and evaporating salts. The unit, which is related to the Quaternary, is seen as old alluvial fans.

The lithology at the Kaviro deposit mainly consists of the middle Jurassic Baghamshah Formation (Fig. 2). The Baghamshah Formation is dominated by marly shale and marl with small contents of gypsum. This unit in the Kaviro deposit is affected by low grade regional metamorphism and has changed into slate. Slate units are dark to black because of abundant organic material that sometimes gives a soapy feeling to the rock. This unit is altered by the ore-fluid reaction in the proximity of the vein. Common gangue minerals in the vicinity of the vein are dolomite and minor amounts of quartz. The local faults have east-west and north-south trends.

The layers of the Baghamshah formation in the Kaviro area are folded in the form of anticlines and synclines. Therefore, the geometric aspects of the folds are summarized below.

These folds have asymmetric profiles and their vergence is to the northwest, indicating approximately NE–SW shortening. The folds are often cylindrical. Inter-limb angle is close and fold hinge is angular to sub rounded. These folds have small amplitudes, and their wavelengths are generally between 150 m to 200 m. The fold axis position is  $117^{\circ}/60^{\circ}$  SW, and axial plane position (calculated using the average orientation of axial plane cleavages) is  $214^{\circ}/77^{\circ}$  NW.

These folds are formed due to movement on steeply dipping reverse and thrust faults. The thrust faults movement orientation is from SE to NW. The average orientation of veins is  $144^{\circ}/90^{\circ}$  and these veins are perpendicular to the fold axis. Individual veins range from 0.1 cm to 1.5 m in thickness and display sub planar to crudely lensoidal form. Due to deformation, these folds have axial plane cleavage on their axial plane. These cleavages are the most pervasively developed planar fabric observed in many field exposures. From intersection of cleavages with bedding surface, pencil structures are formed in parallel to fold axis. Stereonet plots for these intersection lineations, presented by type and by domain, are shown in Fig. 3.

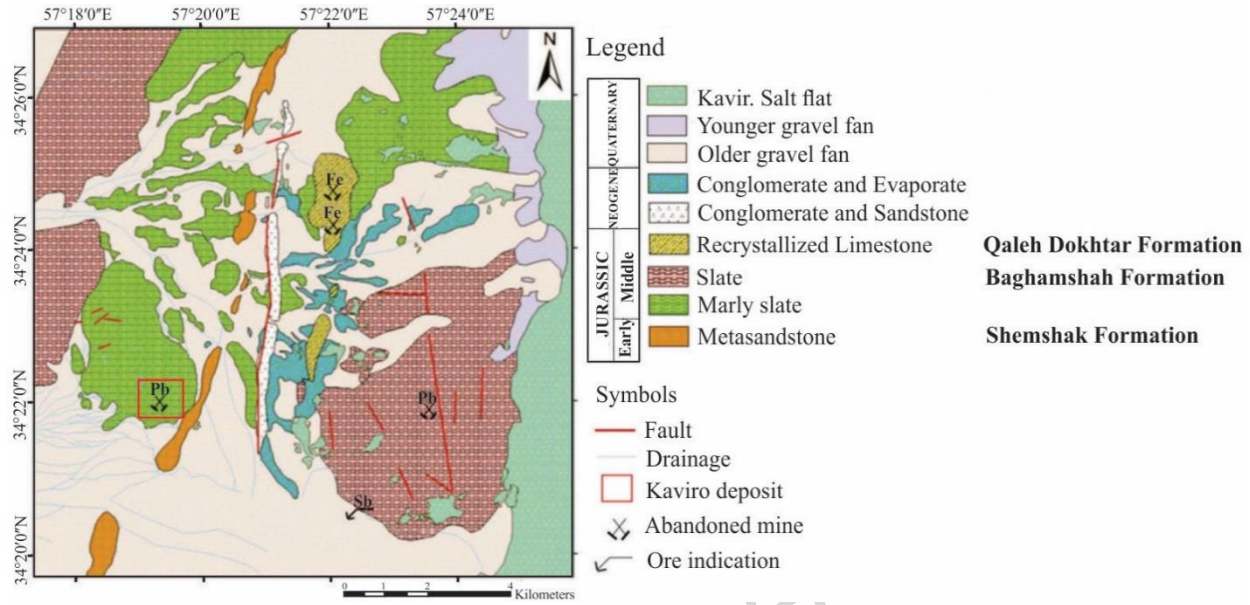


Figure 2. Geological map of the Neyghanan region (modified after Routner et al., 1994).

### 3. Sampling and analytical method

#### 3.1. Ore mineralogy

Forty-two polished and fifteen thin-polished sections were collected from pre-mineralization stage quartz-pyrite veins and also from main stage dolomite-quartz-sulfide veins. The samples were principally collected from trenches and drill holes, and the samples were selected in such a way as to show all the vein types, ranging from mineralized to non-mineralized units.

#### 3.2. Fluid inclusions

The fluid inclusion samples were collected from surface, trenches, and from various depths of drill holes in the ore-bearing vein in the area. Thirteen doubly polished wafers (150  $\mu\text{m}$  thick) (five quartz wafers of pre-mineralization stage coexisting with pyrite and eight dolomite wafers of main stage coexisting with galena) were processed for microthermometric analysis to gain preliminary feedback on the temperatures and salinities of the ore-forming fluid. To distinguish shape, size, phase, distribution pattern and possible origin of fluid inclusions, polished thin sections were checked under transmitted light.

Microthermometric measurements were organized using standard techniques (Roedder, 1958, 1972, 1984) and a Linkam THM 600 heating-freezing stage ( $-190$  to  $600$   $^{\circ}\text{C}$ ) affixed on an Olympus TH4-200 microscope stage at Ferdowsi University of Mashhad, Iran. The accuracy is estimated to be  $\pm 0.2$   $^{\circ}\text{C}$  on freezing,  $\pm 2$   $^{\circ}\text{C}$  below  $350$   $^{\circ}\text{C}$  and approximately  $\pm 4$  above  $350$   $^{\circ}\text{C}$  on

heating. The stage was calibrated at low temperatures with the aid of heptane ( $-90.6\text{ }^{\circ}\text{C}$ ), chloroform ( $-63.0\text{ }^{\circ}\text{C}$ ), chlorobenzene ( $-45.6\text{ }^{\circ}\text{C}$ ), n-dodecane ( $-9.6\text{ }^{\circ}\text{C}$ ) and distilled water ( $0.0\text{ }^{\circ}\text{C}$ ). Calibration at  $45\text{ }^{\circ}\text{C}$  was undertaken via Merck Melting Point standard 9645 and at  $306\text{ }^{\circ}\text{C}$  via sodium nitrate. Salinity of the fluids trapped in fluid inclusions was calculated based on the temperature of final ice melting ( $T_m$ ) and homogenization temperature ( $T_h$ ) using Flnacor software. Densities were calculated using Flnacor software and according to microthermometric data (Brown and Lamb, 1989).

### 3.3. Sulfur isotopes

In the Kaviro deposit, galena was the only appropriate sulfide mineral for isotopic analysis because the amount of sulfur and its microscopic features were suitable. For interpreting the origin and the genesis model of the deposit, the  $\delta^{34}\text{S}$  of galena samples were analyzed. Because the amount of pyrite was too small, the mineral separation and isotopic analyses were not performed.

The galena-bearing samples that were selected for fluid inclusion study and sulfur isotopic analysis show a close relationship with dolomite. Therefore, we can use the measured microthermometric temperature of dolomite for galena. Six samples were collected from drill holes, and one sample was selected from trenches. The samples were crushed and homogenized.

The samples were crushed again in a ceramic mortar and then sieved into four standard sieves with mesh numbers of 10, 16, 18, and 20. Samples with mesh numbers between 18 and 20, which have the most frequent fractions (1 to 0.850 mm), were selected, and the high purity concentrations of galena were handpicked under a binocular microscope.

Isotopic analyses of sulfur for galena samples were performed at Iso-Analytical Ltd., Crewe, Cheshire, United Kingdom. These measurements were performed by Elemental Analysis–Isotope Ratio Mass Spectrometry (EA-IRMS). Isotopic analysis was undertaken according to the monitoring of  $m/z$  48, 49, and 50 of  $\text{SO}^+$  produced from  $\text{SO}_2$  in the ion source. The results ( $\delta^{34}\text{S}$  values) are represented in the standard per mil notation relative to the international Canyon Diablo Troilite (CDT) standard. For quality control, 20 % of the samples were analyzed in duplicate.

### 3.4. Pb isotopes

Five galena samples were analyzed for lead isotopes. All the samples were from drill holes. The lead isotope analyses were performed on galena minerals in an Oslo University lab (Norway). Galenas leached from samples via dilute acid were mixed with phosphoric acid and silica gel and were loaded on an outgassed Re filament. Ratios were measured via thermal ionization mass spectrometry with a MAT262 instrument using multiple Faraday cups in static mode. The data were corrected for 0.10 +/- 0.06 % per atomic mass unit. The reproducibility of the fractionation (based on NBS982) was propagated into the uncertainty of the corrected ratios.

#### 4. Ore deposit

The Kaviro deposit is composed of many small orebodies occurring as veins and veinlets. These orebodies strike 30-40° W and dip 90° (Fig. 3). The veins' average thickness is 25 cm. The average grades are 2.5 % Pb, 20 g/t Ag, 370 g/t Zn, and 450 g/t Cu. The ore minerals are mainly galena and pyrite. The gangue minerals are principally dolomite, quartz and calcite. The structures of the ores can be massive, brecciated, disseminated, vein, or veinlet. The prevalent alteration related to the Pb mineralization are dolomite and quartz assemblages. Crosscutting relationships in the veins indicates that the ore paragenesis of the Kaviro deposit can be divided into three stages: (1) pre-mineralization stage quartz-pyrite, (2) main stage dolomite-quartz-galena-pyrite, and (3) late stage carbonate-pyrite. Of these three stages, the middle stage is the main mineralizing event.

Finally, widespread weathering influenced the superficial levels of the area covering the alteration of the host-rocks. A supergenic stage consisting of secondary minerals (malachite, covellite, hematite, goethite, cerussite and anglesite) was formed during the weathering and oxidation of the ore.

##### 4.1. Texture

Mineralization in the Kaviro deposit mainly occurred in structurally open spaces and much less frequently as a replacement of host rock.

Massive texture is not common in the area and is seen in galena samples restricted to just two boreholes (Fig. 4a). The most common form of open-space filling texture in the Kaviro deposit is brecciation texture. Although host rock brecciation occurs in the Kaviro deposit, it is not a

common sight and is confined to some places (Figs. 4b, c). The brecciated fragments are cemented by a matrix of dolomite, quartz and galena. The breccia clasts range from a few millimeters to a few centimeters in size; they have sharp contacts against their cements and therefore can be considered as a tectonic breccia. Because of the high porosities and permeabilities of tectonic breccias, they are important places for the transmission and deposition of ore fluids. Disseminated texture occurs due to the replacement and/or open-space filling. Disseminated galena or pyrite in host rocks occurs in vicinity of the ore zones. The size of disseminated galena grains vary between 2 mm to 1 cm, and the size of pyrite grains is between 1 mm to 5 mm. These disseminated mineral grains resulted from hydrothermal fluids that penetrated the host rock (Fig. 4d). Replacement texture is seen as dolomitic replacement of slate fragments in brecciated slate. For this texture, calcite minerals in slate fragments are replaced by fine grained dolomite. Framboidal texture is seen in some pyrite samples. For this type of pyrites, framboids are completely round (Fig. 4e). In some cases, these framboids follow each other and show island texture. The framboids have sizes less than 2 mm. This type of texture is seen in the pyrites that are located in slate host rock. Island texture is seldom seen in framboidal pyrites when they follow each other.

#### *4.2. Ore mineralogy*

Galena and dolomite are the main primary minerals. Pyrite and small amounts of residual chalcocite are seen as minor sulfides. In the supergene zone, cerussite ( $\text{PbCO}_3$ ), anglesite ( $\text{PbSO}_4$ ), covellite ( $\text{CuS}$ ), malachite ( $\text{Cu}_2\text{CO}_3(\text{OH})_2$ ), hematite ( $\text{Fe}_2\text{O}_3$ ) and goethite ( $\text{FeO}(\text{OH})$ ) are seen. In addition to the dolomite, the minor gangue minerals are quartz and calcite. Galena has formed approximately 99 % of Kaviro sulfide minerals by volume; the galena crystals are subhedral to anhedral and range from 0.1 to 4 cm across.

##### *4.2.1. Hypogene mineralization*

The generalized paragenesis of mineral association in the Kaviro deposit is shown in Fig. 5. Megascopic and microscopic textural studies of the ore show that hypogene mineralization has taken place during three stages. In the first stage, course grained quartz and pyrite veins are formed (Fig. 4f). In the second stage of ore formation, galena with minor amounts of pyrite, dolomite and fine-grained quartz replaced the host rock (Figs. 4g, h). Finally, course-grained calcite veins occur together with scarcely disseminated and veinlet pyrite cutting the earlier



formed minerals (Fig. 4i). These veins are also seen in the host rock away from the mineralization area, showing a lack of any relationship between mineralization and the formation of these veins.

Galena as anhedral grains are the most abundant ore minerals and is seen as cumulates within a size range of 0.1–4 cm in the ore. This mineral does not include any type of inclusions. Undulation and displacement of the triangular pits indicates that deformation happened after deposition of galena (Malekzadeh Shafaroudi et al., 2015) (Fig. 4j). Galena also developed as small grains in the brecciated zone (Fig. 4k), with some crystals up to 3 mm in size. However, dolomite–quartz–galena veins are seen in the host rock. Cerussite and anglesite are observed mostly as overgrowths that form concentric textures along the borders of galena (Fig. 4l). Small amounts of covellite formed from chalcocite occur at contacts between galena and gangue minerals (Fig. 4l).

Pyrite has minor contribution and occurs as disseminated euhedral and/or subhedral grains (0.2 to 2 mm) and in the form of small veinlets (0.5 to 4 mm thicknesses) in the host rock. This mineral is partly or wholly transformed into goethite.

#### 4.2.2. Supergene mineralization

The position of the water table and its changes, host rock lithology, primary mineralogy, fluid access and its chemistry, and climatic regime are the main factors that influenced the supergene processes (Jeffrey, 2001). Fractures are very abundant in the Kaviro deposit host rock, and therefore the supergene environment is an open system. Therefore, water can continuously reach equilibrium with the atmosphere; in addition, because of the warm and dry climate, biological activities in soil are low, and pH is particularly influenced by host-rock and mineral composition. In the supergene zone, cerussite ( $\text{PbCO}_3$ ), anglesite ( $\text{PbSO}_4$ ), covellite ( $\text{CuS}$ ), malachite ( $\text{Cu}_2\text{CO}_3(\text{OH})_2$ ), hematite ( $\text{Fe}_2\text{O}_3$ ) and goethite ( $\text{FeO}(\text{OH})$ ) are seen. Anglesite and cerussite were formed from galena, and goethite formed from pyrite. The normal covellite with severe pleochroism was commonly observed around the galena (Fig. 4l). Malachite and covellite are seen as minor amounts and are possibly formed from supergene alterations of chalcopyrite.

#### 4.3. Wall rock alteration



Wall-rock alteration in the Kaviro deposit consists of dolomitization (dolomite veins) and silicification (quartz vein). The alteration styles directly related to Pb mineralization are dolomitization (Fig. 6a). These different alteration styles are described briefly below.

4.3.1. Dolomitization: This alteration happened in wall rock as dolomite veins and accompanied vein mineralization as dolomite–galena±quartz veins (mainly with open space filling texture) (Fig. 6b) and/or as the predominant gangue mineral in the matrix of ore-bearing breccia with lesser amounts of quartz. Dolomites, which are seen as a dolomite cement of brecciated slates, have planar faces, are less than 20  $\mu\text{m}$  in diameter and in some cases are accompanied with fine grained quartz. The dolomite is predominantly zoned and ranges from white to cream. Field observations were combined with petrographic identification of size, shape, and zoning and with the dolomite occurrence's relationship to ore mineralization in the Kaviro deposit. This multipronged progress permitted the detection of two types of dolomite, as follows.

Fine crystalline dolomites (Dol-1), which are less than 20  $\mu\text{m}$  in diameter, are common as a cement, with galena infilling the slate fragments in tectonic breccia. The amount of galena accompanied by this type of dolomite is rare (Figs. 4c, 6c).

Coarse crystalline dolomite (saddle dolomite, Dol-2), the crystals of which are as wide as 1 mm in diameter, are unimodal and nonplanar with curved edges. Saddle dolomite is often paragenetically connected with galena mineralization in veins (Fig. 6d). Ore minerals and saddle dolomite are commonly intergrown. These features promote the interpretation that the saddle dolomite is cogenetic with the ore minerals.

Most fluctuations in growth banding and zoning in various hydrothermal dolomite crystals show successive differences in the physico-chemical conditions of the fluid transporting various quantities of  $\text{Fe}^{2+}$ ,  $\text{Mn}^{2+}$ , and trace elements (Fraser et al., 1989). Fast changes in Mn/Fe ratios and  $f\text{O}_2$  of the hydrothermal fluid forced the dolomite zonation in the Kaviro deposit.

4.3.2. Silicification: Silicification occurred in wall rock as quartz-pyrite±calcite veins and sometimes is seen as a gangue mineral in the matrix of ore-bearing breccia (Figs. 6a, d). Quartz was formed in two distinct stages: pre-mineralization stage coarse grained quartz is accompanied

by pyrite and main stage fine grained quartz is accompanied by saddle dolomite and galena (Fig. 4f).

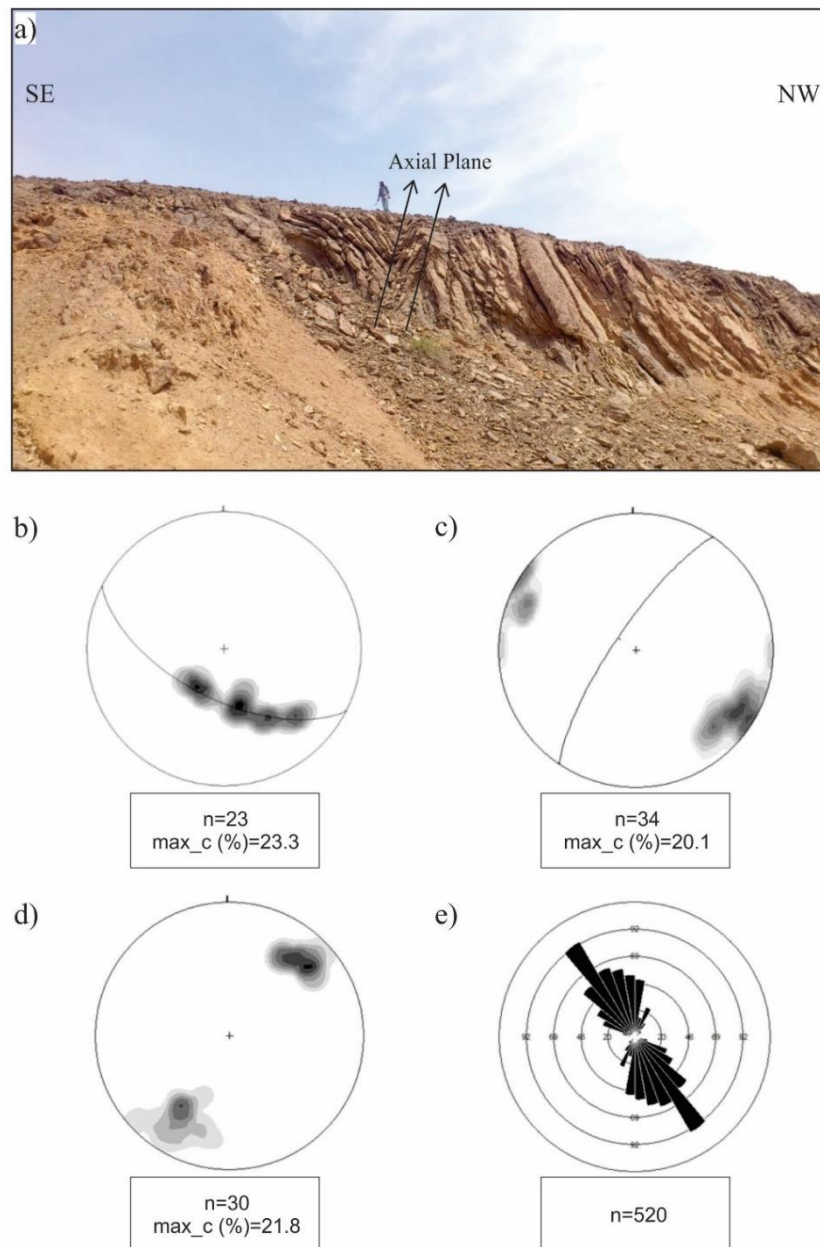


Figure 3. (a) Field image of folding in Baghamshah formation. Lower hemisphere equal area projections, (b) contoured poles to bedding in the Baghamshah Formation. The great circle represents best fit and the pole to great circle which indicates the calculated fold axis, (c) contoured poles to axial plane cleavage, the great circle represents the average orientation of axial plane cleavages which indicates the calculated axial plane, (d) contoured poles to pencil

structures which is formed due to the intersection of cleavages with bedding surface, and (e) rose diagram showing the trend of the measured hydrothermal veins in the Kaviro deposit.

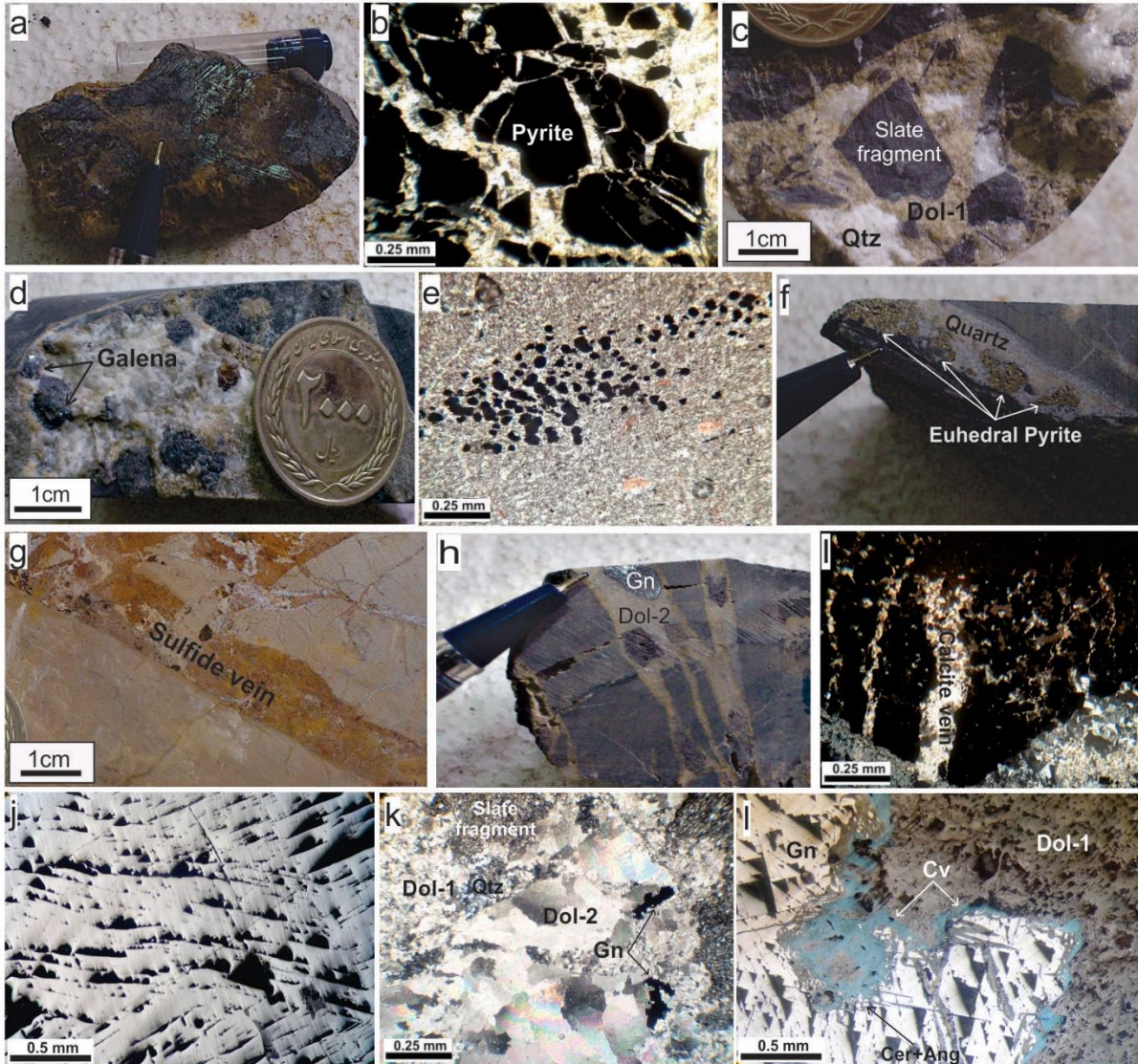


Figure 4. Photographs illustrating the textural characteristics of the Kaviro deposit. (a) massive to crystalline galena of the main vein; (b) brecciated pyrite which show tectonic events in the area; (c) brecciated slate with dolomite and quartz cements; (d) disseminated galena grains; (e) framboidal pyrite in slate host rock; (f) quartz-pyrite vein from pre mineralization stage; (g) sulfide vein of the main stage of mineralization; (h) dolomite- galena veinlet from main stage with open space filling texture; (i) calcite vein of the late stage crosscutting Pb ore of the main stage; (j) undulation of the triangular pits in galena; (k) galena and dolomite as the cement of



brecciated slate unit; (l) secondary minerals in the border of galena. Abbreviations: Dol, dolomite; Gn, galena; Py, pyrite; Cer, cerussite; Ang, anglesite; Cv, covellite; (Whitney and Evans, 2010).

Minerals	Pre-Mineralization Stage	Main Mineralization Stage	Post-Mineralization Stage	Supergene Mineralization Stage
Dolomite		High		
Calcite	High		High	
Quartz	High	Medium		
Galena		High		
Pyrite	High	Medium		
Chalcocite		Very Low		
Cerussite				High
Anglesite				High
Covellite				Very Low
Malachite				Very Low
Hematite				High
Goethite				High





High  Medium  Low  Very Low 

Figure 5. The paragenetic sequence of the Kaviro lead deposit.

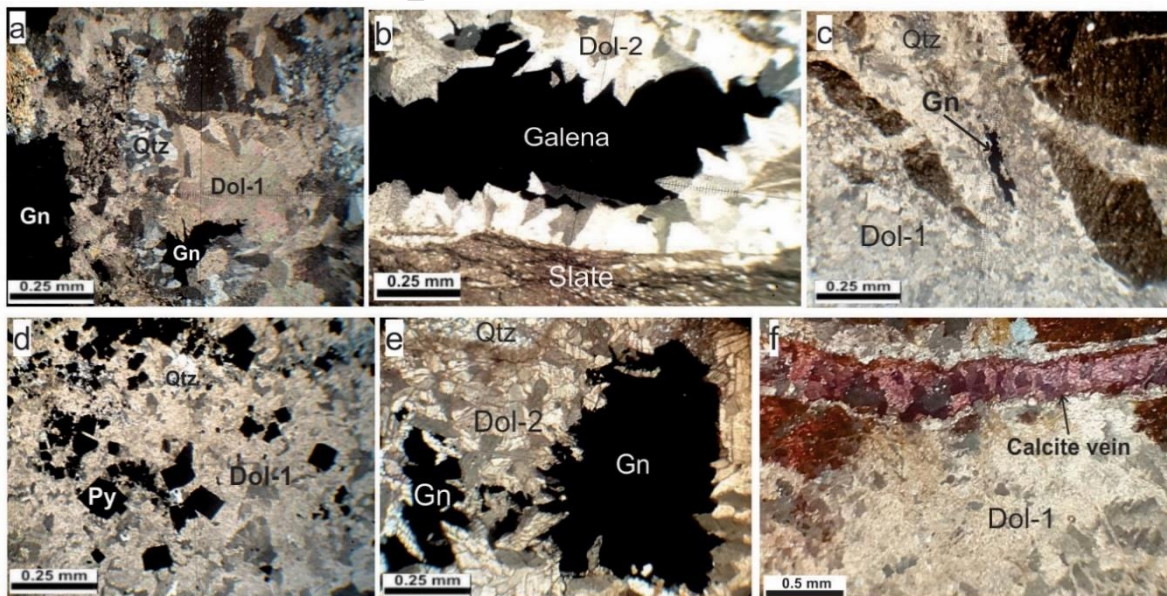


Figure 6. Photomicrographs of alteration types in the Kaviro lead deposit: (a) dolomitization alteration as dolomite and minor quartz; (b) dolomite-galena vein; (c) fine-grained dolomite (Dol-1) with quartz and galena in brecciated zone; (d) fine-grained dolomite (Dol-1) with pyrite and quartz; (e) saddle dolomite (Dol-2) with galena and calcite; (f) late colored calcite vein cutting the dolomite vein. Abbreviations: Dol, dolomite; Gn, galena; Qtz, quartz; Py, pyrite (Whitney and Evans, 2010).

## 5. Fluid inclusions

### 5.1. Petrography and morphology of fluid inclusions

Petrographic examinations of fluid inclusions in quartz of pre-mineralization stage accompanied with pyrite and dolomite of main mineralization stage accompanied with galena were implemented to determine the hydrothermal fluid characteristics and to assess the composition of the ore-forming fluids. Secondary fluid inclusions were commonly readily distinguished under low power magnification in clearly defined planes that cut across or terminate at grain boundaries. Primary fluid inclusions were searched for in areas where secondary planes were not abundant and were distinguished on the basis of criteria given by Roedder (1984). The key attributes used to determine primary fluid inclusions were (1) isolation from other inclusions, (2) the random distribution of inclusions (not on planar features), and (3) inclusions that typically follow growth zones. Petrographic studies in both dolomite and quartz samples showed two types of fluid inclusions: 1) liquid only (L) inclusions, which are rare, and 2) liquid-vapor (L-V) inclusions.

Fluid inclusions were scattered as clusters, single inclusions, and along fractures or grain boundaries. Primary fluid inclusions (with minor secondary fluid inclusions) are dominant in dolomite and quartz samples and are interpreted as representing the fluids existing at the time of hydrothermal mineral growth. These primary fluid inclusions were defined by trapping during crystal growth, but the secondary inclusions occurred as fracture-controlled arrays after the growth of the host crystal (Roedder, 1984; Van den Kerkhof and Hein, 2001). Primary fluid inclusions are abundant in small size (typically 2 to 11  $\mu\text{m}$  and averaging 6  $\mu\text{m}$ ) in dolomite samples, whereas quartz includes primary fluid inclusions of larger size (typically 3 to 13  $\mu\text{m}$  and averaging 7  $\mu\text{m}$ ) (Fig. 7 and Table 1). Fine-grained quartz crystals occurring at the vein with

dolomite and galena do not contain primary fluid inclusions requiring study. Most of the fluid inclusions are elliptical, rod-shaped, round, or irregular.

At room temperature, all of the measured inclusions are considered primary because they are restricted within special growth zones of the host mineral (Roedder, 1984). The type of inclusions in both dolomite and quartz are two-phase, liquid-rich and contain a vapor bubble that generally occupies 5 up to 15 % volume of the inclusion cavity that homogenizes into a liquid state upon heating (Fig. 7), indicating that fluids were homogeneous (miscible) at the time of trapping. The absence of liquid CO<sub>2</sub> or clathrate formation during freezing experiments suggests that none of the inclusions included significant quantities of CO<sub>2</sub>. Although many measurements were achieved, no fluid inclusion evidence for a fluid boiling process in the Kaviro samples was observed because FI along growth zones, FI trapped at the same time, all show equal volumetric phase ratios (Goldstein and Reynolds, 1994; Bodnar, 2003).

### *5.2. Microthermometric measurements*

Microthermometric measurements were undertaken on the primary two-phase (L-V) inclusions larger than 5 µm in diameter. Only heating analysis was performed on the inclusions that were very small.

Homogenization temperature ( $T_h$ ) values range from 180 to 220 °C (average 199 °C, n=88) in dolomite and 210 to 250 °C (average 224 °C, n=45) in quartz (Table 1 and Fig. 8a). These  $T_h$  values show a minimum temperature of trapping of the hydrothermal fluid in an inclusion. The specific pressure during mineralization is unknown in the area. On the other hand, no boiling process is seen in the fluid inclusions. Dolomite and galena show a close relationship with another. Microthermometric measurements show that the deposit can be considered to be a medium- to low-temperature deposit (Malekzadeh Shafaroudi and Karimpour, 2015; Jazi et al., 2016).

Freezing analyses reveal that the first melting temperature ( $T_{fm}$ ) values of primary inclusions in both dolomite and quartz crystals cluster between -60 and -55 °C (average -58 °C, n=85). Comparing the values to the eutectic temperatures of different water-salt systems (Shepherd et al., 1985; Gokce, 2000) suggests that they show hydrothermal fluids that include salts of CaCl<sub>2</sub>, MgCl<sub>2</sub>, and NaCl. The  $T_{fm}$  temperature irregularities are possibly due to the presence of salts,

such as MgCl. The hydrothermal dolomite alteration of host rocks indicates the presence of Mg in the ore-forming fluids. The presence of carbonates and quartz in the veins suggests that the fluid's pH was somewhat acidic. Under situations such as this and through such elevated chloride activities, it is most probable that metal-chloride complexes were the main species responsible for transporting Pb (Sverjensky, 1987).

No difference in  $T_{fm}$  was detected between the samples taken from surface and drill holes; this exhibits that the salt composition of the fluid was homogenous during earlier and later mineralizing events. Salt types and their compositions may be as a result of circulation of the mineralizing fluid through middle Jurassic sedimentary rocks.

The final ice melting temperatures ( $T_{m,ice}$ ) values range from  $-3.2$  to  $-6.5$  °C (average  $-5.2$  °C,  $n=55$ ) in dolomite and  $-5.2$  to  $-8.9$  °C (average  $-7.3$  °C,  $n=30$ ) in quartz (Table 1 and Fig. 8b). Salinities (wt.% NaCl equivalent) of ore-forming fluids can be calculated by the relationship between final ice melting temperatures and salinities (Hall and Sterner 1988). The salinities of the hydrothermal fluids were calculated using the equation by Bodnar (1993), and yielded wt.% NaCl equivalents as follows: 5.1 to 9.8 wt.% NaCl equivalent (average 8.2 wt.% NaCl equivalent,  $n=55$ ) in dolomite and 8 to 12.5 wt.% NaCl equivalent (average 10.7 wt.% NaCl equivalent,  $n=30$ ) in quartz (Table 1 and Fig. 8c).

Mean salinity values of primary inclusions in dolomite and quartz show that the salinity of the mineralizing fluids was slightly higher during quartz precipitation in the earliest stage and was decreased through later stages of mineralization (dolomite precipitation) (Fig. 8c). These salinity data indicated that the ore-forming fluids were medium- to low-salinity fluids. The density of ore-forming fluids can be calculated using the equation proposed by Brown and Lamb (1989), and the densities in this study range from 0.91 to 0.98 g/cm<sup>3</sup> (average value of 0.93 g/cm<sup>3</sup>,  $n=55$ ) in dolomite and 0.91 to 0.97 g/cm<sup>3</sup> (average value of 0.93 g/cm<sup>3</sup>,  $n=30$ ) in quartz (Table 1 and Fig. 8d).

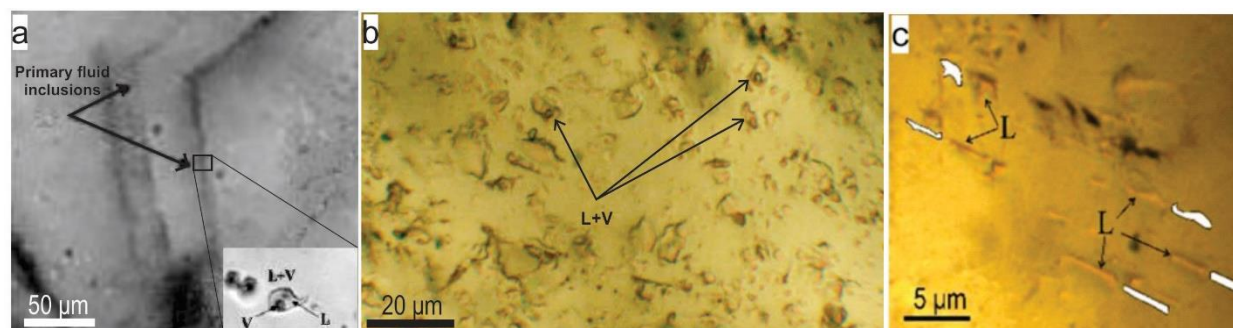


Figure 7. Photomicrographs of primary fluid inclusions in quartz and dolomite in the Kaviro lead deposit. (a) liquid–vapor inclusions along growth zones in the quartz of pre-mineralization stage, (b) liquid–vapor inclusions in the dolomite of main mineralization stage, and (c) liquid inclusions in the dolomite of main mineralization stage.

Table 1. Microthermometric data of primary fluid inclusions in the Kaviro deposit.

Sample no.	Host mineral	Number	$T_h$ (°C)	$T_{m,ice}$ (°C)	Salinity (NaCl wt. % equiv.)	Density (g/cm <sup>3</sup> )
<b>BH16-6</b>	Dolomite	10	180-203	−4.9 to −6.1	7.7-9.3	0.93-0.94
<b>BH1-9</b>	Dolomite	15	185-219	−5.4 to −6.5	8.3-9.8	0.92-0.95
<b>BH4-1</b>	Dolomite	9	184-198	−3.2 to −3.9	5.2-6.6	0.91-0.93
<b>BH10-5</b>	Dolomite	15	193-220	−4.3 to −5.7	7.5-8.7	0.91-0.93
<b>P11</b>	Dolomite	12	185-215	-	-	-
<b>P1</b>	Dolomite	15	187-220	-	-	-
<b>BH1-5</b>	Dolomite	6	184-193	−5.4 to −6.4	8.4-9.7	0.96-0.99
<b>BH10-11</b>	Dolomite	7	194-207	-	-	-
<b>BH4-1</b>	Quartz	8	210-221	−5.2 to −6.1	8.1-9.3	0.91-0.92
<b>BH15-3</b>	Quartz	13	209-247	−6.9 to −8.7	10.3-12.5	0.91-0.94



<b>BH2-11</b>	Quartz	6	220-244	-	-	-
<b>P17</b>	Quartz	9	210-220	-	-	-
<b>P5</b>	Quartz	9	227-250	-6.9 to -8.9	10.3-12.5	0.92-0.97
<b>Pre mineralization stage deposited quartz (average)</b>			222	-7.1	10.6	0.93
<b>Main stage deposited dolomite (average)</b>			199	-5.2	8.2	0.93

$T_h$ , homogenization temperature;  $T_m$ , temperature for final ice melting.

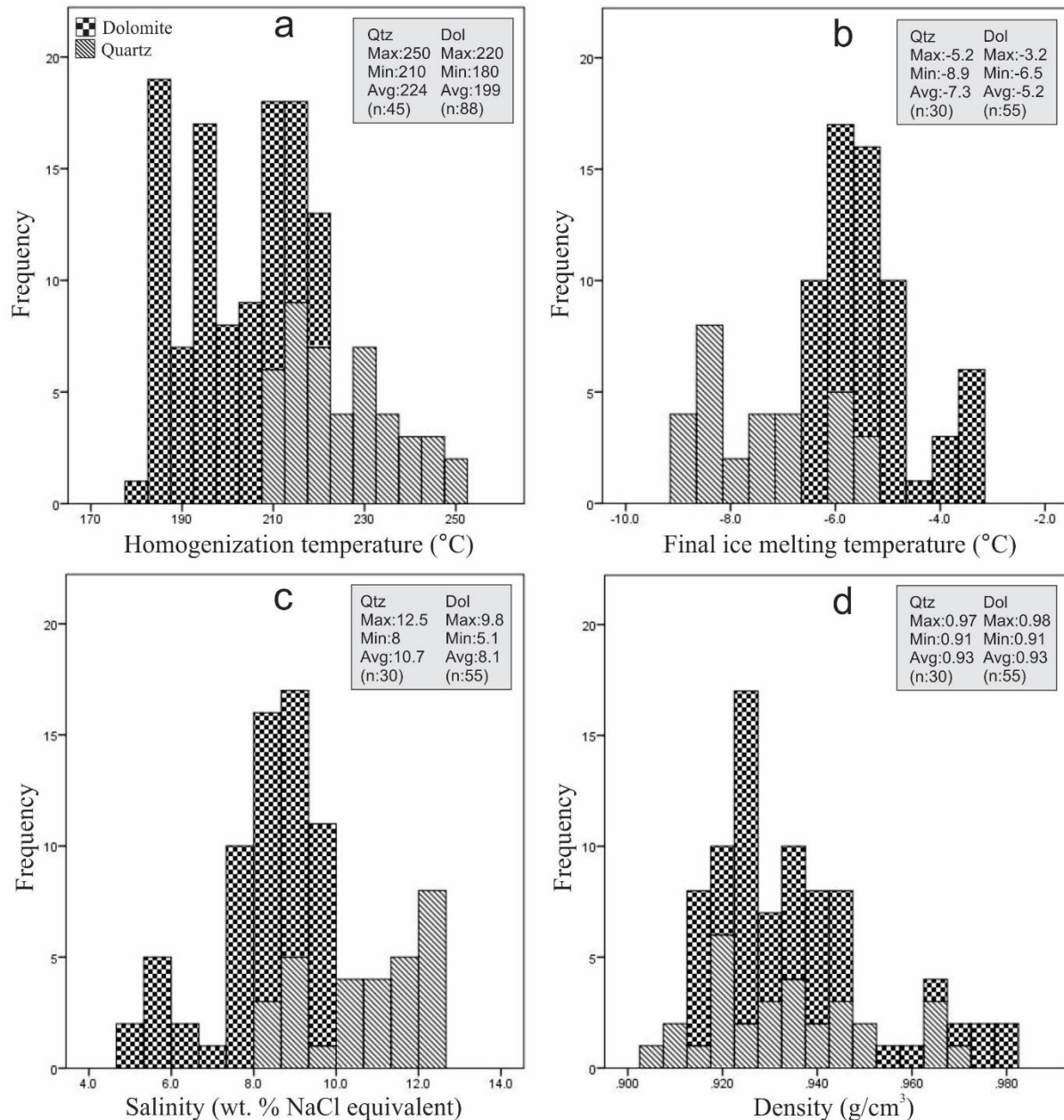


Figure 8. Histogram showing the thermodynamic data of primary fluid inclusions in the Kaviro deposit. (a) Homogenization temperature (°C) histogram, (b) Final ice melting temperature (°C) histogram, (c) Salinity (wt.% NaCl equivalent) histogram, and (d) Density (g/cm<sup>3</sup>) histogram.

## 6. Sulfur isotopes

The isotopic compositions of sulfur ( $\delta^{34}\text{S}$  values) in sulfide minerals and/or mineralizing fluid ( $\delta^{34}\text{S}_{\Sigma\text{S}}$ ) in the sulfide-bearing deposits enable us to better understand both possible sources of

sulfur and other metallogenic elements. Sulfur isotopes are useful tools for realizing the formational conditions of sulfur-bearing minerals in ore deposits (Ohmoto, 1972; Ohmoto and Goldhaber, 1997). A number of factors mainly control the isotopic composition of sulfur in hydrothermal minerals and include the  $fO_2$  and pH values of the hydrothermal fluids, its temperature, and the isotopic composition of the sulfur in the mineralizing fluids (Ohmoto, 1972).

The S isotopic compositions of galena samples from the veins at the Kaviro deposit are summarized in Table 2. The  $\delta^{34}S$  values of the seven galena samples were  $-1.86\text{‰}$  to  $+0.69\text{‰}$  and averaged  $-0.66\text{‰}$ . The original fluid  $\delta^{34}S_{H_2S}$  can be estimated from the  $\delta^{34}S$  values of the hydrothermal ore minerals. The  $\delta^{34}S$  values of galena occupy a narrow range and were slightly depleted in  $^{34}S$ . According to the physical and chemical conditions ( $T < 300^\circ\text{C}$ , low pH and Eh), expect for the vein fluids, the main sulfur species would be  $H_2S$  (Ohmoto and Rye, 1979). The predominance of sulfide at these temperatures causes sulfide mineral  $\delta^{34}S$  values to be close to the original fluid  $\delta^{34}S_{H_2S}$  (Ohmoto and Rye, 1979).

The primary fluid  $\delta^{34}S_{H_2S}$  values in equilibrium with galena were estimated to a range between  $+0.94\text{‰}$  to  $+3.27\text{‰}$  (average,  $+2.28\text{‰}$ ) (Fig. 9). This explanation, according to the equation proposed by Li and Liu (2006), was gained by evaluating the  $\delta^{34}S$  values of galena and the average temperature of the hydrothermal fluid during the galena mineralization period ( $186^\circ\text{C}$ – $206^\circ\text{C}$ , obtained by homogenization temperature consideration during fluid inclusion studies in the dolomite samples that have a close relationship with galena) (Table 2).

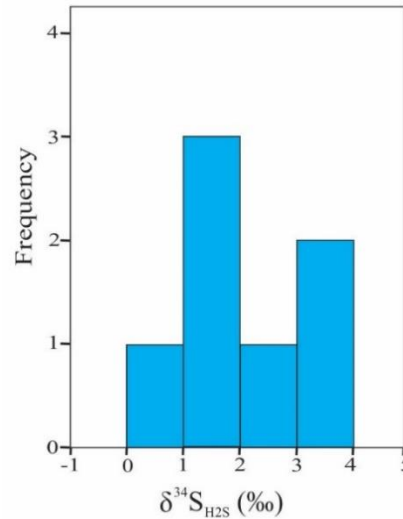


Figure 9. Histogram of  $\delta^{34}\text{S}_{\text{H}_2\text{S}}$  in equilibrium with galena at a certain temperatures (based on the average temperature of the hydrothermal fluid during the galena mineralization period as 186-206 °C, using the Li and Liu (2006) equation).

Table 2: Sulfur isotopic compositions of the Kaviro deposit

Sample no.	Depth (m)	Mineral	Sulfur Content (%)	$\delta^{34}\text{S}_{\text{sulfide}}$ (‰) <sub>CDT</sub>	Th (°C) (fluid calculated)	1000 ln $\alpha$ (Li and Liu, 2006)	$\delta^{34}\text{S}_{\text{H}_2\text{S}}$ (‰)
BH1-4	53	Galena	12.05	0.27	186	-3	+3.27
BH1-9	65	Galena	-	-1.86	204	-2.8	+0.94
BH1-12	80	Galena	-	-0.10	204	-2.8	+2.7
BH4-1	45	Galena	-	0.69	187	-3.0	+3.69
BH10-5	54	Galena	11.34	-1.28	206	-2.8	+1.52
BH10-9	50	Galena	11.34	-1.29	198	-2.9	+1.61
P3	-	Galena	11.99	-1.09	201	-2.8	+1.71

## 7. Lead isotope

Pb isotopes are effective geochemical radioisotopes for understanding ore genesis and for the exploration of mineral deposits demonstrating the crustal evolution (Gulson, 1986; Lu et al., 2000). They are especially useful in assessing the source of metals, providing main information about the nature of Pb reservoir(s), constraining the timing of Pb removal from its source, and defining a geotectonic environment for ore deposits (Gariépy and Dupre, 1991). Galena (PbS) is

the most appropriate mineral for analysis of Pb isotope ratios within Zn-Pb deposits because it is basically free of U and is characterized by an abundant Pb content (~87 wt.%); this combination guarantees that its Pb isotopic composition remains fixed throughout the geologic time.

The results of the Pb-isotope analyses for the five galena samples are provided in Table 3. The  $^{206}\text{Pb}/^{204}\text{Pb}$ ,  $^{207}\text{Pb}/^{204}\text{Pb}$ , and  $^{208}\text{Pb}/^{204}\text{Pb}$  ratios of the samples span narrow ranges of 18.514–18.569 (average of 18.539), 15.668–15.715 (average of 15.689), and 38.803–38.950 (average of 38.869), respectively.

Pb isotope research is principally used to confine the probable source rocks of the metals in deposits. When the isotope data are plotted on Stacey and Kramers' (1975) model curves for average crustal Pb-isotope evolution, the  $^{207}\text{Pb}/^{204}\text{Pb}$  and  $^{208}\text{Pb}/^{204}\text{Pb}$  ratios plot above the evolution curves and clearly show a crustal source (Figs. 10a, b). Possible Pb sources also have been checked using the plumbotectonic diagrams of Zartman and Haines (1988) (Fig. 10a). In Fig. 10a, the  $^{207}\text{Pb}/^{204}\text{Pb}$  vs.  $^{206}\text{Pb}/^{204}\text{Pb}$  data cover an area near and above the Upper Crust curve, suggesting a homogen source for the Pb.

In the  $^{208}\text{Pb}/^{204}\text{Pb}$  vs.  $^{206}\text{Pb}/^{204}\text{Pb}$  diagram (Fig. 10b), all samples plot above the upper crust, mantle, and orogen average values, showing a major contribution of Th-derived lead.

Table 3: Lead-isotope composition of the analyzed samples in the Kaviro deposit.

Sample	$^{206}\text{Pb}/^{204}\text{Pb}$	$^{207}\text{Pb}/^{204}\text{Pb}$	$^{208}\text{Pb}/^{204}\text{Pb}$	Model age (Ma)
ZK7-1	18.569	15.715	38.950	279
ZK1-12	18.514	15.668	38.803	225
ZK1-14	18.524	15.677	38.832	234
ZK2-5	18.536	15.689	38.869	249
ZK10-9	18.552	15.700	38.895	260

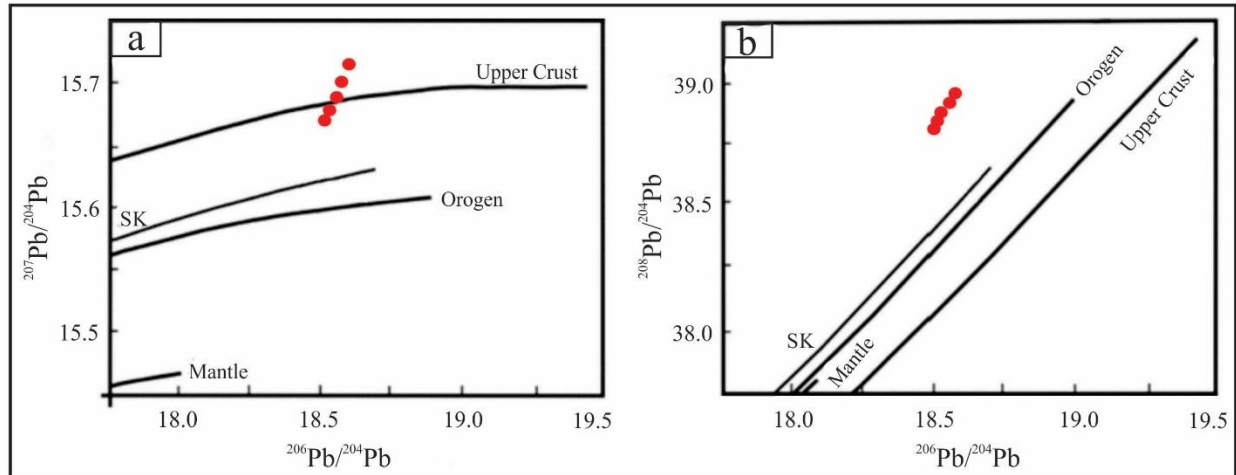


Figure 10. Pb isotope ratios of galena samples in the Kaviro deposit on a ‘plumbotectonic’ diagram (Zartman and Doe, 1981) and Stacey and Kramers (SK) curve (1975).

## 8. Discussion

### 8.1. Evolution of ore-forming fluids

The importance of isotopic analyses in illustrating the possible source of hydrothermal fluids is represented by many studies (Albinson et al., 2001; Wilkinson, 2001; Criss and Farquhar, 2008). The predominant sulfide ores within the Kaviro deposit are galena, and there are minor amounts of pyrite. The  $\delta^{34}\text{S}$  values in the galena veins range from  $-1.86\text{‰}$  to  $+0.69\text{‰}$  (average  $-0.66\text{‰}$ ), and the range of estimated  $\delta^{34}\text{S}_{\text{H}_2\text{S}}$  is between  $+0.94\text{‰}$  to  $+3.27\text{‰}$  (average  $+2.28\text{‰}$ ). Based on the absence of sulfate minerals in the veins, transporting of sulfur was in a reduced state.

The values of S ( $+0.94\text{‰}$  to  $+3.27\text{‰}$ ) do not show a particular source for sulfur. According to Figure 11, magmatic, sedimentary, or metamorphic sources could be the major sources of sulfur for mineralization. Based on the absence of an intrusive body around the Kaviro deposit, a magmatic source is excluded.

Consistently, the low salinity contents of fluid inclusions argue against a magmatic source for fluids. When the sedimentary rocks are the origin of sulfur,  $^{34}\text{S}$ -depleted sulfur commonly results, but the average of  $\delta^{34}\text{S}_{\text{H}_2\text{S}}$  in the Kaviro deposit is  $+2.28\text{‰}$  and sedimentary rocks could not be the source of sulfur. Oxygen and hydrogen isotope data are required to be able to further discuss the source of the ore fluids.

Our analyses of fluid inclusions of the Kaviro lead deposit exposed that the ore-forming fluids were medium–low temperature and medium-low salinity H<sub>2</sub>O–NaCl system fluids. The pressure–temperature diagram of Fournier (1999) revealed that the pressure during formation of the Kaviro deposit was approximately <1 MPa, which is equivalent to a depth of approximately <1 km, assuming hydrostatic and lithostatic pressure (Fig. 12). Therefore, the vein was formed at shallow depth, as confirmed by the structure and texture of the ore minerals.

Ore-forming hydrothermal fluids generally transport metals in complexes with aqueous Cl<sup>-</sup> and HS<sup>-</sup> (Barnes, 1979). The mechanisms leading to the precipitation of metals from Cl<sup>-</sup> and/or HS<sup>-</sup> complexes are composed of the following (Barnes, 1979; Ramboz et al., 1982; Robb, 2004; Chi and Xue, 2011): (1) temperature decrease, (2) pressure decrease, (3) phase separation, (4) fluid mixing/dilution, and (5) fluid/rock interaction causing pH and Eh shifts.

Fluid inclusion studies show that there is a close relationship between homogenization temperature and salinity (e.g., Shepherd et al., 1985; Wilkinson, 2001). Chemical compositions of typical hydrothermal fluids can be plotted in a homogenization temperature vs. salinity diagram that aids in determining the type of hydrothermal system and deposit (Kesler, 2005). On the fluid evolution diagram (Fig. 13), homogenization temperature indicates a positive correlation with fluid salinity. Former investigations have indicated that homogenization temperature and fluid salinity, as well as fluid salinity and enthalpy, show positive correlation with the process of fluid mixing, whereas the data show negative correlation trends during fluid boiling (Shepherd et al., 1985). According to the evidence provided for fluid mixing outlined by Zhang (1997), the aspects of fluid evolution of the Kaviro deposit are consistent with a fluid-mixing scenario. Specifically, the salinity-homogenization temperature diagram showed a fluid evolution trend shifting from relatively high (primary fluid inclusions in quartz accompanied with pyrite) to relatively low (primary fluid inclusions in dolomite accompanied with galena) homogenization temperature and salinity (Fig. 13). The homogenization temperature and salinity of the mineralizing fluids were higher (210–250 °C) during quartz precipitation in the earliest stage and were reduced through later stages of mineralization (180–220 °C in dolomite precipitation) (Fig. 13). This salinity content proposes mixing of hydrothermal solutions (metamorphic fluids) with meteoric water, according to Wilkinson (2001). A decrease in the salinity contents of fluid inclusions due to mixing with meteoric water has also been recognized

in similar studies (Breskovska and Tarkian, 1993; Dolnicek et al., 2009; Huizenga et al., 2006). It is well known that mixing can play a definitive role in interpreting the origin and formation of large hydrothermal ore deposits (Zhu et al., 2001; Cooke and McPhail 2001; Fan et al., 2011; Gu et al., 2011; Zhai et al., 2013). Fluid mixing has played an important function in the Kaviro deposit. Taking into account the undiscovered plutonic intrusion in close proximity to the Kaviro deposit (in the 1:100000 map of Eshghabad that Neyghanan is part of, we do not observe any intrusive body), we suggested that the metals and sulfur in the deposit were most likely derived from the surrounding sedimentary rocks. We have IP/RS data at 90 m depth, but magnetometry has not yet been undertaken.

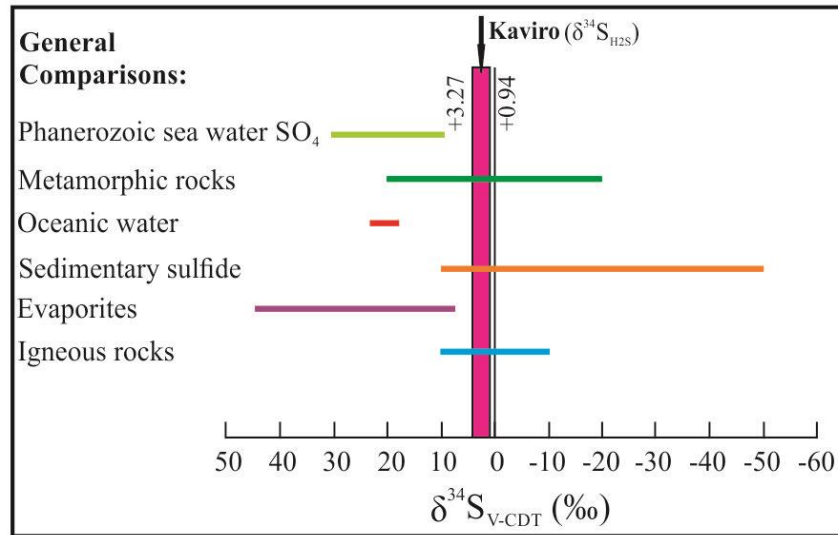


Figure 11: The value of  $\delta^{34}\text{S}_{\text{H}_2\text{S}}$  in the Kaviro deposit compared with  $\delta^{34}\text{S}$  in different geological setting (Hoefs, 1988).



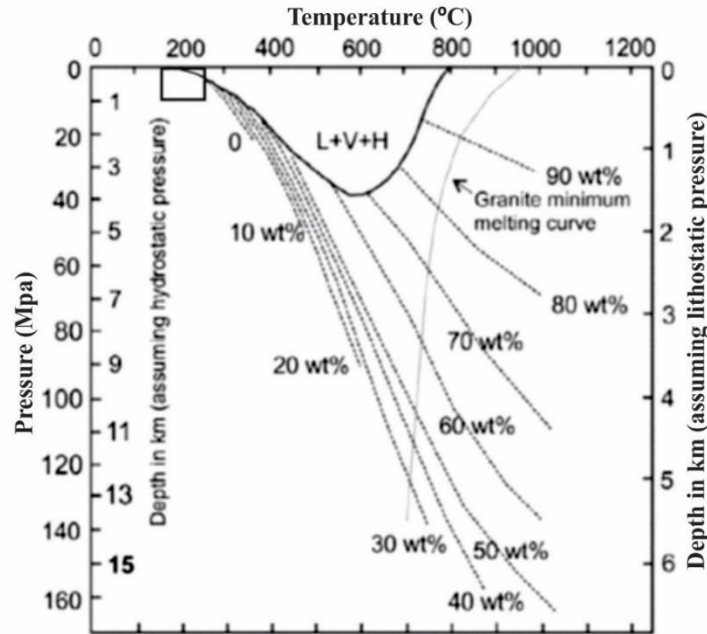


Figure 12. Pressure–temperature diagram illustrating phase relationships in the NaCl-H<sub>2</sub>O system at lithostatic and hydrostatic pressures (Fournier, 1999). L = liquid, V = vapor, H = halite. Thin dashed lines are contours of constant wt. percent NaCl dissolved in brine. Filled gray line indicates granite minimum melting curve. Filled dark line shows the three-phase boundary, L+V+H, for the system NaCl-KCl-H<sub>2</sub>O with Na/K in solution fixed by equilibration with albite and K-feldspar at the indicated temperatures. Rectangle shows the location of dolomite and quartz fluid inclusions.

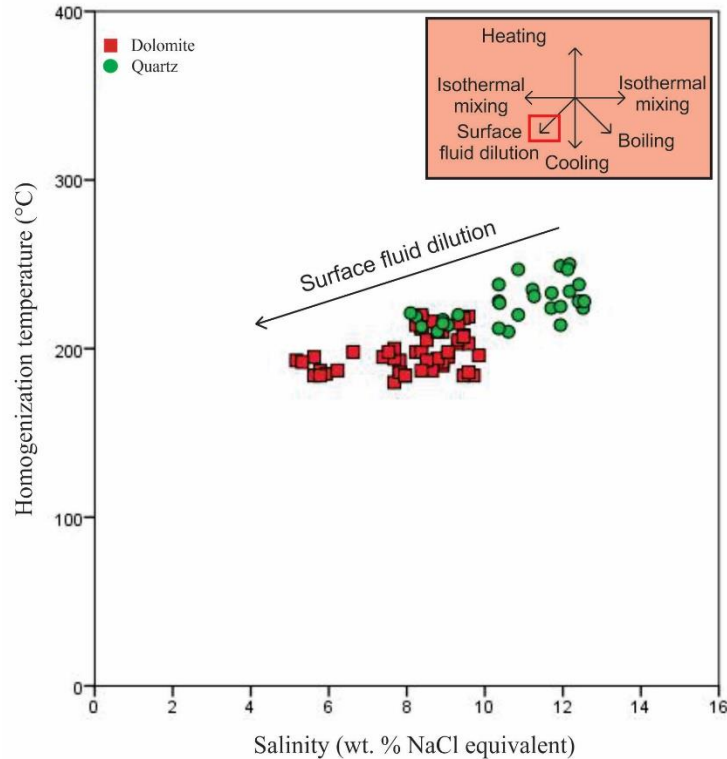


Figure 13. Schematic diagram showing typical trends in homogenization temperatures salinity space due to various fluid evolution processes (after Wilkinson, 2001).

### 8.2. Mineralization model and genetic type

The Lut Block has a large potential for porphyry Cu and Cu-Au, related-epithermal Au, and Cu-Pb-Zn vein-type deposits due to its past subduction zone between the Lut and the Afghan Blocks (Malekzadeh Shafaroudi, 2009; Karimpour et al., 2011). A few detailed studies have been of note regarding genetic model and formation of base-metal deposits in the Lut Block (Lotfi, 1982; Mehrabi and Talefazel, 2011; Mehrabi et al., 2011; Mirzaei Rayeni et al., 2012; Malekzadeh Shafaroudi and Karimpour, 2013b). The Kaviro deposit is one of the many Pb-Zn vein deposits and is found in the Lut block. A geologic and genetic relation between ore vein and middle Jurassic regional metamorphism is evident. On the basis of the widespread regional metamorphism, vein mineralization, and the features of ore deposit geology, we expect the formation of the Kaviro deposit to be directly linked to regional metamorphism of the middle Jurassic and/or at a few subsequent times. Coupled with late-stage addition of meteoric water, these fluids created favorable conditions for the metallogenic elements to accumulate and precipitate during the formation of this ore deposit. During the middle Jurassic and afterwards,

low-grade regional metamorphism in the Kaviro region brought about generation of a series of vein mineralization. In addition, faults and folds were organized due to these severe tectonic and metamorphic activities. Folds are asymmetric and cylindrical, and their axial plane position is  $214^{\circ}/77^{\circ}$  NW. These folds are formed due to movement on steeply dipping reverse and thrust faults. The thrust faults' movement orientation is from SE to NW.

The early fluids, which had relatively high temperature and salinity and aided in the development of quartz-pyrite veins of early stage, were formed by regional metamorphic activity. Ore forming fluids ascended along appropriate structures (reverse faults) and deposited in folds. In addition, the fluids seem to have ascended to a sufficiently shallow depth to allow for efficient fluid mixing with meteoric water.

Through the reaction of relatively hot fluids with wall rock and heat recharge by geothermal anomalies in the region, the meteoric water, which initially had relatively low temperature and salinity, might have extracted significant amounts of metallogenic materials from host rock. Through mixing between fluids of different characteristics and metal contents, these combined fluids changed the conditions of the ore-forming fluid system, disturbing the chemical equilibrium of solutions, initiating main chemical reactions, and finally causing precipitation from solution of metallogenic materials during the formation of this ore deposit.

Accordingly, fluid mixing seems to indicate an important mechanism for explaining the formation of the Kaviro deposit. In addition, the genetic type of the Kaviro lead deposit is categorized as a metamorphic-related vein deposit.

On the other hand, the computed  $\mu(^{238}\text{U}/^{204}\text{Pb})$  values for 5 galena samples using the Pb-isotope model of Stacey and Kramers (1975) range from 9.9 to 10.1 ( Fig. 14). The  $\mu$  values in the mantle and crust are 8.92 and 9.58, respectively (Doe and Zartman, 1979). The  $\mu$  values of metal sulfides from the Kaviro deposit are between 9.9 and 10.1, which are evidently higher than the range of 8–9 in the mantle and 9.58 in the crust (Doe and Zartman, 1979), expressing that Pb was principally derived from the crust. These values suggest that the Pb is predominantly derived from rocks with high U/Pb ratios, characteristic of the Upper Crust (Zartman and Doe, 1981). Since the Pb-isotope data of possible source rocks in the region are not available, the eventual source(s) of Pb is unclear.

The calculated ages using the Pb-isotope model of Stacey and Kramers (1975) range from 279 to 225 Ma (average 249.4 Ma), indicating a Permian to Triassic age (Table 3). The ages from the model that point to pre-middle Jurassic origin imply that galena mineralization was derived from remobilization of lead from an earlier reservoir in the Permian or Triassic units, either from the host rocks themselves or from earlier-formed ore deposits within those units.

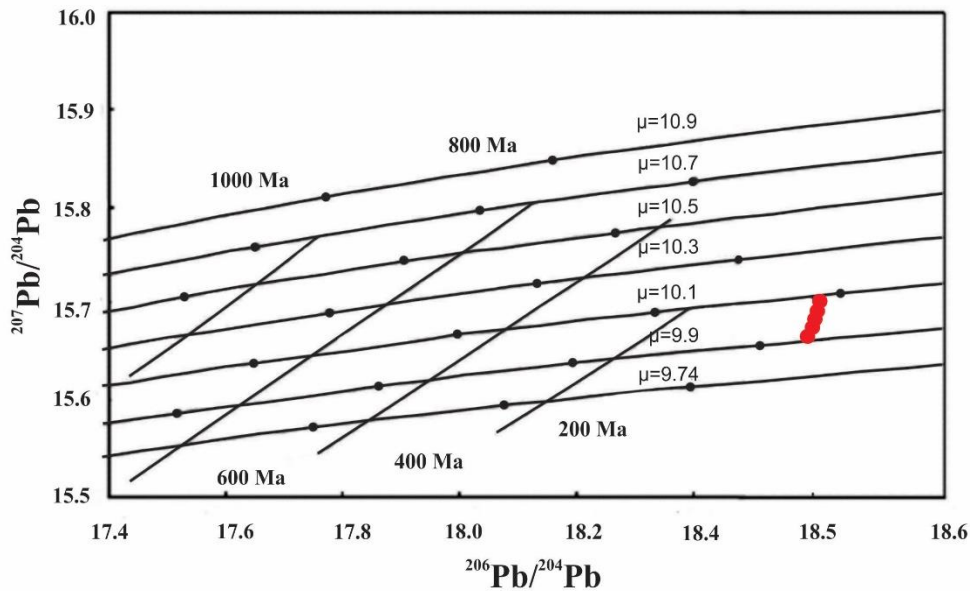


Figure 14.  $\mu$  values of galena samples (red dots) are plotted on evolution growth curve of Stacey and Kramers (1975). The black dots correspond to the age for each step used to calculate the growth curves and the straight lines are Pb-Pb isochrons.

### 8.3. Comparison of average Pb isotope ratios in Kaviro and selected Pb-Zn deposits in the Central Iranian Microcontinent

The CIM is a complex tectonic region and is the largest geological unit in Iran. Because of persistent convergence between the Arabian and Turan plates, continuous continental deformation is seen in this region.

The early tectonic evolution that shaped the CIM is determined by Proto-Tethyan. Two more episodes of orogenic events that impact the CIM were in the Early Triassic and in the Late Tertiary (Stöcklin, 1974). During the Paleozoic, the CIM was stable, but this platform was deformed by the late Triassic movements (Zanchi et al., 2009). The structural trends appeared in

the Mesozoic when the continuous platform of the CIM was separated into small parts (Stöcklin, 1968; Ramezani and Tucker, 2003). There are many Pb-Zn deposits in the CIM that frequently occur in carbonate rocks of the Paleozoic–Tertiary, especially in Cretaceous carbonates (Table 4).

Table 5 lists the Pb isotope ratios of galena samples from 6 selected Pb-Zn deposits within CIM (Mirnejad et al., 2015) (including the Kaviro deposit). The ratios of  $^{206}\text{Pb}/^{204}\text{Pb}$ ,  $^{207}\text{Pb}/^{204}\text{Pb}$ , and  $^{208}\text{Pb}/^{204}\text{Pb}$  are variable and determine the following ranges, respectively: 18.427–19.081, 15.638–15.722, and 38.575–38.910.

All the samples in Figure 15a plot above the model curve for average crustal Pb isotope evolution (Stacey and Kramers, 1975) and do not show any systematics. In addition, the Pb isotope data in 3 samples (Mehdiabad, Nakhlak, and Chahsorb) plot between the ‘Orogen’ and ‘Upper crust’ growth curves of Zartman and Doe (1981; Figure 15a), and the others (Kamarmehdi, Geyjerkuh, and Kaviro) plot above the upper crust curve.

The samples that plot between the orogen and upper crustal growth curves in the  $^{207}\text{Pb}/^{204}\text{Pb}$  vs.  $^{206}\text{Pb}/^{204}\text{Pb}$  plumbotectonic diagram (Figure 15a) may show multiple sources for Pb during orogenic events. However, the high ratios of  $^{207}\text{Pb}/^{204}\text{Pb}$  (15.638–15.689) for sedimentary-hosted deposits (Mehdiabad, Nakhlak, Chahsorb, and Kaviro) may show a greater contribution of old crust or pelagic sediments. In Figure 15b ( $^{208}\text{Pb}/^{204}\text{Pb}$  vs.  $^{206}\text{Pb}/^{204}\text{Pb}$  diagram), all the samples, except Kamarmehdi, plot above the upper crust, mantle, and orogen mean values, indicating a major contribution of Th-derived lead (Mirnejad et al., 2015). The main specifics of the Chahsorb and Kaviro deposits are the extensive presence of thick sediments of the Shemshak Formation (Upper Triassic-Lower Jurassic) beneath the host rocks and the influence of tectonic events (e.g., thickening of the crust and orogenic activities) in Pb mineralization. A previous study in the Chahsorb region considered the Shemshak Formation as a probable source of metals and suggested that mineralization occurred following the extraction of ore-bearing fluids from Shemshak shales during crustal thickening and orogenic phases (Pourabdollahi 2009). Galena samples hosted by sedimentary rocks are characterized by higher  $\mu$  ( $^{238}\text{U}/^{204}\text{Pb}$ ) ratios (9.8 to 10.1) (Table 5) when compared to galena samples in the igneous rocks, and this may be ascribed to higher contributions of upper crustal sources.

According to the Pb isotope data shown in Figure 16, it is obvious that the ore-forming fluids in all deposits hosted by sedimentary rocks, except Kamarmehdi, are of nonmagmatic sources.

Table 4: Summary of the selected Pb-Zn deposits in the CIM.

Number	Deposit name	Location	Geologic relationship and host rock	Ore and gangue type	Ore type	reference
1	Nakhlak	53°50'10"E 33°34'30" N	fault and fracture infilling, massive, brecciated minerals and breccia cements in Cretaceous carbonate	Galena (ore), barite, calcite, and dolomite (gangue)	MVT	(Jazi et al., 2017)
2	Chahsorb	56°39'02" N 34°03'15" E	Strata-bound, vein, karst and open-space infilling in Jurassic limestone and dolomitic limestone	Galena (ore), calcite, quartz, and barite (gangue)	MVT	(Pourabdollahi, 2009)
3	Kamarmehdi	56°30'14" E 32°02'06" N	Fault infilling and brecciated zone in Triassic carbonates	Galena (ore), fluorite, calcite, dolomite, and quartz (gangue)	Epithermal	(Sadeghibojd, 1995)
4	Geyjerkuh	56°58'25" E 31°53'28" N	Fault and fracture infilling within Permian–Triassic(?) carbonate	Sphalerite, galena (in deep parts of deposit), and oxide and carbonate minerals of Zn-Pb in upper part of deposit (ore), barite, calcite, and quartz (gangue)	MVT?	(Mirnejad et al., 2015)
5	Mehdiabad	54°01'30"E 31°29'03" N	Infilling of faults and fractures, massive, brecciated minerals and breccia cements of in lower Cretaceous carbonate	Sphalerite, galena, and other Zn-Pb carbonates and oxide minerals (ore), barite, and calcite (gangue)	Eastern part of deposit is similar to MVT and the central and western parts are	(Ghasemi, 2007). (Hitzman et al., 2003; Reichert, 2007)

					similar to Irish type	
6	Kaviro	57°19'19" E 34°22'19" N	Open space and Fracture infilling in middle Jurassic low metamorphosed shale	galena (in deep parts of deposit), and oxide and carbonate minerals of Pb and Fe in upper part of deposit (ore), dolomite, calcite, and quartz (gangue)	Vein type	this paper

Table 5: Isotopic compositions of Pb in Pb-Zn deposits of the Central Iranian Microcontinent (CIM) (Mirnejad et al., 2015).

Deposit name	$^{206}\text{Pb}/^{204}\text{Pb}$	$^{207}\text{Pb}/^{204}\text{Pb}$	$^{208}\text{Pb}/^{204}\text{Pb}$	$\mu (^{238}\text{U}/^{204}\text{Pb})$	Model age (Ma)
Nakhlak	18.516	15.638	38.641	9.8	162
Chahsorb	18.427	15.647	38.575	9.9	246
Kamarmehdi	19.081	15.722	38.910	10.1	-82
Geyjerkuh	18.514	15.704	38.696	10.1	297
Mehdiabad	18.499	15.658	38.634	9.9	215
Kaviro	18.538 (average)	15.689 (average)	38.869 (average)	10.0 (average)	249 (average)

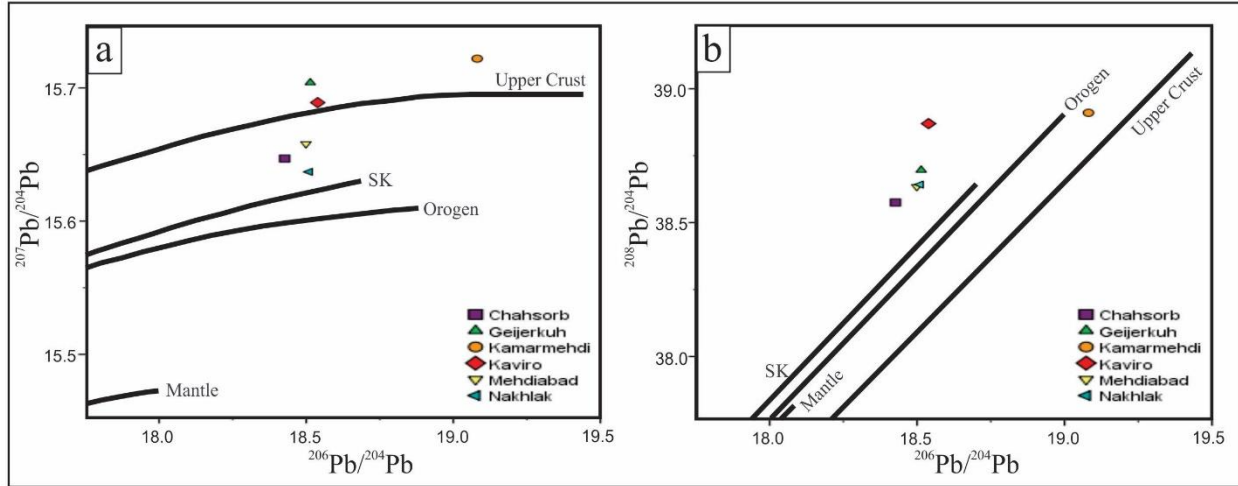


Figure 15: Isotopic ratios of Pb in galena samples from selected deposits in the Central Iran zone (CIM) on a 'plumbotectonic' diagram (Zartman and Doe, 1981) and Stacey and Kramers (SK) curve (1975).

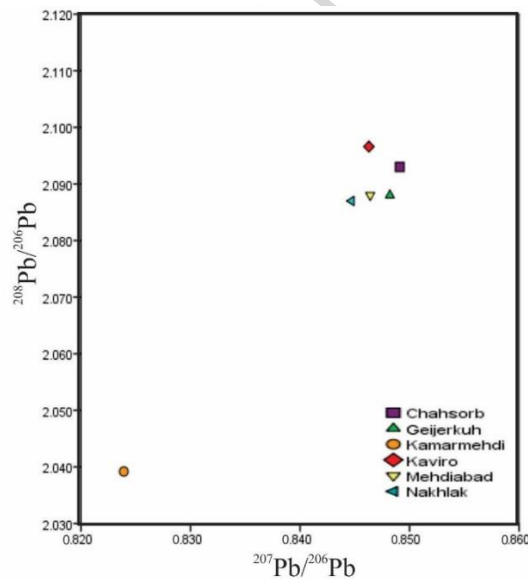


Figure 16: Diagram showing the  $^{208}\text{Pb}/^{206}\text{Pb}$  vs.  $^{207}\text{Pb}/^{206}\text{Pb}$  ratios in the Kaviro deposit and other Pb-Zn deposits in the CIM.

## 9. Conclusions

(1) The Kaviro lead deposit occurred in an area sealed by middle Jurassic rocks in the northwestern Lut Block. The distribution of ore bodies within the area was primarily controlled by folds. The alteration zone is marked by an assemblage of dolomite, quartz and calcite. The ore



vein includes galena with minor pyrite as hypogene minerals and cerussite, anglesite, covellite, malachite, and goethite as secondary minerals. Dolomite and quartz are the dominant gangue minerals.

(2) Three different stages of hypogene mineralization were recognized. The mineral association, paragenesis and textural properties at the microscopic and macroscopic scales were found to be similar in the investigated ore locations.

(3) Fluid inclusion data revealed that the ore-forming fluids included significant amounts of divalent cations ( $\text{CaCl}_2$  and  $\text{MgCl}_2$ ) along with NaCl. Microthermometric studies and composition measurements of fluid inclusions indicated that the general characteristics of the ore-forming fluids involved medium- to low-temperature and medium- to low-salinity in the NaCl- $\text{H}_2\text{O}$  system. These findings showed that the mineralization developed within the hydrothermal system. The positive correlation between the homogenization temperature and fluid salinity, combined with the ore deposit geology, provide proof that aqueous mixing was the main process in the evolution of the ore-forming fluids.

(4) The values of  $\delta^{34}\text{S}$  in galena samples from the Kaviro deposit ranged between  $-1.86\%$  to  $+0.69\%$ . The  $\delta^{34}\text{S}_{\text{H}_2\text{S}}$  values in equilibrium with galena were calculated to be in the range of  $+0.94\%$  to  $+3.27\%$  (average  $+2.28\%$ ). The possible source of sulfur could be explained by derivation from a metamorphic source by leaching of sulfides from the slate units.

(5) The Pb isotopic compositions of galena separated from the Kaviro lead deposit showed that Pb was derived from a source with high, time-integrated U/Pb and Th/Pb ratios. For the deposit investigated here, the Pb isotope data plotted around the 'upper crust' growth curve (Zartman and Doe, 1981), suggesting that Pb was derived from a continental crust source.

(6) The formation of the Kaviro Pb ore deposit was controlled by hydrothermal fluids related to the middle Jurassic and/or regional metamorphic activity in the Lut Block a short time later.

(7) The isotopic composition of Pb in galena samples from the CIM Pb-Zn deposits reveal that Pb was derived from sources with high U/Pb and Th/Pb ratios. A mixed source (continental crust and mantle) is proposed for Pb when the amount of Pb isotopic data plots between the 'upper crust' and 'orogen' growth curves (Zartman and Doe, 1981). In most deposits, the calculated

model ages show the Mesozoic age. Therefore, it is possible that Pb was derived from the source(s) in the CIM and is related to orogenic activities during the Mesozoic. Two parameters that played important roles in Pb remobilization and deposition of Pb-Zn mineralization in the host rocks are tectonic activities and crustal thickening (Mirnejad et al., 2015).

In conclusion, the lead isotope data combined with geological, structural, and petrographic information suggest that a long-term duration of focused circulation of metamorphic fluids that mainly leached metals from the basement rocks ascending upward through reverse faults that cut up through the stratigraphy and thrust the Baghamshah Series over itself. Because of this thrust and reverse fault movement, folding occurred. These folds are suitable locations for vein mineralization. In terms of the genetic type of deposit, the Kaviro deposit is classified as a metamorphic-related vein deposit (Fig. 17). Prospecting for new deposits should be concentrated in the Lut Block.

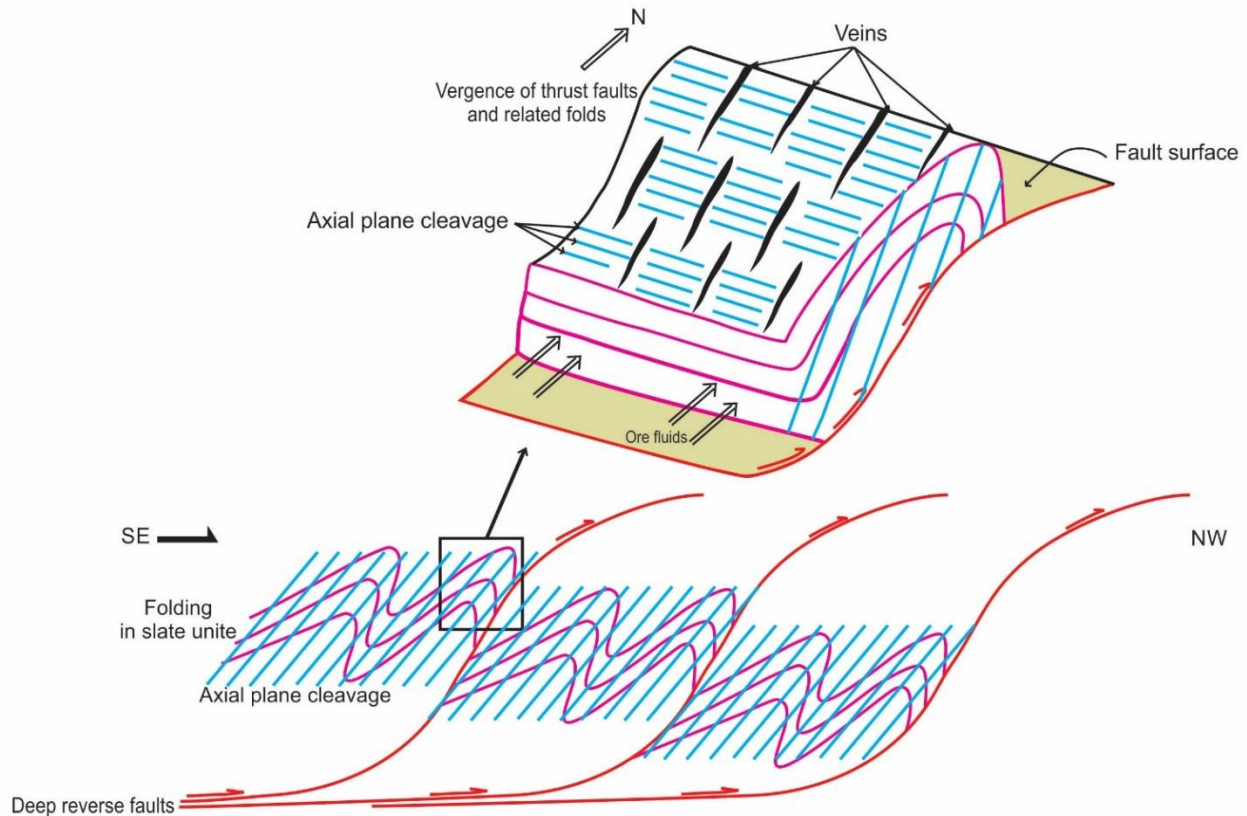


Figure 17. Schematic cartoon illustrating the model for the development of the fault–fold system and associated hydrothermal mineralization at Kaviro. It is suggested that ascending ore-bearing

fluids are passed through steeply dipping thrust and inverse faults and continually focused into the anticline and trapped into extensional veins.

### Acknowledgements

The Research Foundation of Ferdowsi University of Mashhad, Iran, supported this study (Project No. 27128). FC received support from a Smaaforsk grant of the University of Oslo. Thanks to the anonymous reviewers for their constructive and helpful reviews of this manuscript.

### References

- Agard, P., Monié, P., Gerber, W., Omrani, J., Molinaro, M., Meyer, B., Labrousse, L., Vrielynck, B., Jolivet, L., and Yamato, P., 2006. Transient, synobduction exhumation of Zagros blueschists inferred from P–T, deformation, time, and kinematic constraints: implications for Neotethyan wedge dynamics. *J. Geophys. Res.* 111, B11401, <https://doi.org/10.1029/2005JB004103>
- Agard, P., Omrani, J., Jolivet, L., Whitchurch, H., Vrielynck, B., Spakman, W., Monie, P., Meyer, B., and Wortel, R., 2011. Zagros orogeny: A subduction-dominated process: *Geological Magazine* 148, 692–725, [https://doi: 10.1017/S001675681100046X](https://doi:10.1017/S001675681100046X).
- Aghanabati, A., 2004. *Geology of Iran*. Geological Survey of Iran, 600 p.
- Alavi, M., 1994. Tectonics of the Zagros orogenic belt of Iran: new data and interpretations. *Tectonophysics* 229, 211-238, [https://doi.org/10.1016/0040-1951\(94\)90030-2](https://doi.org/10.1016/0040-1951(94)90030-2)
- Albinson, T., Norman, D.I., Cole, C., Chomiak, B., 2001. Controls on formation of low-sulfidation epithermal deposits in Mexico: constraints from fluid inclusion and stable isotope data. *Society of Economic Geologists Special Publication* 8, 1-32.
- Arjmandzadeh, R., 2011. Mineralization, geochemistry, geochronology, and determination of tectonomagmatic setting of intrusive rocks in Dehsalm and Chahshaljami deposits, Lut Block, eastern Iran. Ph.D. Thesis Ferdowsi University of Mashhad 215 (in Persian).

Arjmandzadeh, R., Karimpour, M.H., Mazaheri, S.A., Santos J F, Medina J M and Homam S M 2011 Sr-Nd isotope geochemistry and petrogenesis of the Chah-Shaljami granitoids (Lut Block, eastern Iran). *J. Asian. Earth Sci.* 41, 283-296, <https://doi.org/10.1016/j.jseaes.2011.02.014>

Arjmandzadeh, R., Santos, J.F., 2014. Sr-Nd isotope geochemistry and tectonomagmatic setting of the Dehsalm Cu-Mo porphyry mineralizing intrusives from Lut Block, eastern Iran. *Int. J. Earth Sci.* 103(1), 123-140, <https://doi.org/10.1007/s00531-013-0959-4>

Bagheri, S., Stampfli, G.M., 2008. The Anarak, Jandaq and Poshte-Badam metamorphic complexes in Central Iran: New geological data, relationships and tectonic implications. *Tectonophysics* 451, 123-155, <https://doi.org/10.1016/j.tecto.2007.11.047>

Barnes, H.L., 1979. Solubilities of ore minerals. In: Barnes H L (Ed.), *Geochemistry of Hydrothermal Ore Deposits* Wiley New York, pp. 404-460, <https://doi.org/10.1017/S0016756800034452>

Bazargani-Guilani, K., Nekouvaht Tak, M.A., Faramarzi, M., 2011. Pb-Zn deposits in Cretaceous carbonate host rocks, northeast Shahmirzad, central Alborz, Iran. *Aust. J. Earth Sci.* 58, 297-307, <https://doi.org/10.1080/08120099.2011.556664>

Berberian, M., 1976. Seismotectonic map of Iran (1:2,500,000). Geological Survey of Iran Press.

Berberian, M., 1977. Historical seismicity map of Iran (1:5,000,000). Geological Survey of Iran Press.

Berberian, F., Berberian, M., 1981. Tectono-plutonic episodes in Iran. *American Geophysical Union Geodynamic Series*. Geological Society of America, Boulder, Colorado 3, 5-33.

Berberian, M., King, G.C.P., 1981. Towards a paleogeography and tectonic evolution of Iran. *Can. J. Earth Sci.* 18, 210-265, <https://doi.org/10.1139/e81-019>

Berberian, M., Yeats, R.S., 1999. Patterns of historical earthquake rupture in the Iranian plateau. *Bull. Seismol. Soc. Am.* 89, 120-139.

- Besse, J., Torcq, F., Gallet, Y., Ricou, L.E., Krystyn, L. and Saidi, A., 1998. Late Permian to Late Triassic palaeomagnetic data from Iran: constraints on the migration of the Iranian block through the Tethyan Ocean and initial destruction of Pangaea. *Geophysical Journal International* 135, 77-92.
- Bodnar, R.J., 1993. Revised equation and table for determining the freezing point depression of H<sub>2</sub>O–NaCl solutions. *Geochim. Cosmochim. Acta* 57, 683-684, [https://doi.org/10.1016/0016-7037\(93\)90378-A](https://doi.org/10.1016/0016-7037(93)90378-A)
- Bodnar, R.J., 2003. Introduction to fluid inclusions. In I. Samson, A. Anderson, & D. Marshall, eds. *Fluid Inclusions: Analysis and Interpretation*. Mineral. Assoc. Canada, Short Course 32, 1-8.
- Breskovska, V., Tarkian, M., 1993. Mineralogy and Fluid inclusion study of polymetallic veins in the madjarovo ore field, Eastern Rhodope, Burgaria. *Mineral. Petrol.* 49, 103-118.
- Brown, P.E., Lamb, W.M., 1989. P–V–T properties of fluids in the system H<sub>2</sub>O ± CO<sub>2</sub> ± NaCl: new graphic presentations and implications for fluid inclusion studies; *Geochim. Cosmochim. Acta* 53, 1209-1221, [https://doi.org/10.1016/0016-7037\(89\)90057-4](https://doi.org/10.1016/0016-7037(89)90057-4)
- Camp, V., Griffis, R., 1982. Character, genesis and tectonic setting of igneous rocks in the Sistan suture zone, eastern Iran. *Lithos* 15, 221-239, [https://doi.org/10.1016/0024-4937\(82\)90014-7](https://doi.org/10.1016/0024-4937(82)90014-7)
- Chi, G.X., Xue, C.J., 2011. An overview of hydrodynamic studies of mineralization. *Geoscience Frontiers* 2, 423-438, <https://doi.org/10.1016/j.gsf.2011.05.001>
- Cooke, D.R., McPhail, D.C., 2001. Epithermal Au–Ag–Te mineralization, Acupan, Baguio district, Philippines: numerical simulations of mineral deposition. *Econ. Geol.* 96, 109-131, <https://doi.org/10.2113/gsecongeo.96.1.109>
- Criss, R.E., Farquhar, J., 2008. Abundance, notation, and fractionation of light stable isotopes. *Rev. Mineral. Geochem.* 68, 15-30, <https://doi.org/10.2138/rmg.2008.68.3>
- Davoudzadeh, M., Schmidt, K., 1984. A review of the Mesozoic paleogeography and paleotectonic evolution of Iran. *J. Mineral. Geochem.* 168(2-3), 182-207.

Doe, B.R., Zartman, R.E., 1979. Plumbotectonics of the Phanerozoic, In: Barnes, H.L. (Ed.), *Geochemistry of Hydrothermal Ore Deposits*. John Wiley, New York, pp. 22-70.

Doglioni, C., Tonarini, S., Innocenti, F., 2009. Mantle wedge asymmetries and geochemical signatures along W- and E-NE directed subduction zones. *Lithos* 113, 179-189, <https://doi.org/10.1016/j.lithos.2009.01.012>

Dolnicek, Z., Fojt, B., Prochaska, W., Kucera, J., Sulovsky, P., 2009. Origin of the Zalesi U-Ni-Co-As-Ag/Bi deposit, Bohemianmasif, Czech Republic: fluid inclusion and stable isotope constraints. *Miner. Depos.* 44, 81-97.

Ehya, F., Lotfi, M., Rasa, I., 2010. Emarat carbonate-hosted Zn-Pb deposit, Markazi Province, Iran: a geological, mineralogical and isotopic (S, Pb) study. *J. Asian Earth Sci.* 37, 186-194, <https://doi.org/10.1016/j.jseaes.2009.08.007>

Fan, H.R., Hu, F.F., Wilde, S.A., Yang, K.F., Jin, C.W., 2011. The Qiyugou gold-bearing breccia pipes, Xiong'ershan region, central China: fluid-inclusion and stable-isotope evidence for an origin from magmatic fluids. *Int. Geol. Rev.* 53, 25-45, <https://doi.org/10.1080/00206810902875370>

Fournier, R.O., 1999. Hydrothermal processes related to movement of fluid from plastic into brittle rock in the magmatic-epithermal environment. *Econ. Geol.* 94, 1193-1212, <https://doi.org/10.2113/gsecongeo.94.8.1193>

Forster, H., 1978. Mesozoic-Cenozoic metallogensis in Iran. *J. Geol. Soc. London* 135, 443-455, <https://doi.org/10.1144/gsjgs.135.4.0443>

Fraser, D.G., Feltham, D., Whiteman, M., 1989. High-resolution scanning proton microprobe studies of micron-scale trace element zoning in a secondary dolomite: implications for studies of redox behavior in dolomites. *Sediment. Geol.* 65, 223-232, [https://doi.org/10.1016/0037-0738\(89\)90024-9](https://doi.org/10.1016/0037-0738(89)90024-9)

Garipey, C., Dupre, B., 1991. Pb isotopes and crust-mantle evolution. In: Heaman L. and Ludden J. N. eds. *Application of Radiogenic Isotope-Systems to problems in geology*. Short course handbook. Mineralogical association of Canada, Toronto, Chapter 6, 191-224.

Geological Survey of Iran, 1989. 1:2,500,000 Geological Map of Iran. Tehran, Geological Survey of Iran, 1 Sheet.

Geological Survey of Iran, 2009. 1:5,000,000 International Geological Map of the Middle East, 2nd ed. Tehran, Geological Survey of Iran, 1 Sheet.

Ghasemi, M., 2007. The genesis of Mehdiabad Zn-Pb deposit and comparison with others Cretaceous Pb-Zn deposits of around Mehdiabad [M.Sc. thesis]. Research Institute of the Geological Survey of Iran, 238 p.

Ghazanfari, F., 1993. Zn-Pb Mines and Deposits in Iran [M.Sc. thesis]. University of Tehran, 199 p.

Ghazi, A.M., Hassanipak, A.A., Mahoney, J.J., Duncan, R.A., 2004. Geochemical characteristics,  $^{40}\text{Ar}$ - $^{39}\text{Ar}$  ages and original tectonic setting of the Band-e-Zeyarat/Dar Anar ophiolite, Makran accretionary prism, S.E. Iran. *Tectonophysics* 393, 175-196, <https://doi.org/10.1016/j.tecto.2004.07.035>

Ghorbani, M., 2002. An introduction to economic geology of Iran. National Geosciences Database of Iran. Report No. 2, 695 (in Farsi).

Gilg, H.A., Boni, M., Balassone, G., Allen, C.R., Banks, D., Moore, F., 2006. Marble-hosted sulfide ores in the Angouran Zn-(Pb-Ag) deposit, NW Iran: Interaction of sedimentary brines with a metamorphic core complex. *Miner. Depos.* 41, 1-16, <https://doi.org/10.1007/s00126-005-0035-5>

Gokce, A., 2000. Ore Deposits. Cumhuriyet University Publication 100, 1-336.

Goldstein, R.H., Reynolds, T.J., 1994. Systematics of Fluid Inclusions in Diagenetic Minerals. USA, Society for Sedimentary Geology, Society of Economic Paleontologists and Mineralogists Short Course 31, 199 p.

Golonka, J., 2004. Plate tectonic evolution of the southern margin of Eurasia in the Mesozoic and Cenozoic. *Tectonophysics* 38, 235-273, <https://doi.org/10.1016/j.tecto.2002.06.004>

- Gu, L.X., Wu, C.Z., Zhang, Z.Z., Franco, P., Ni, P., Chen, P.R., Xiao, X.J., 2011. Comparative study of ore-forming fluids of hydrothermal copper–gold deposits in the lower Yangtze River Valley, China. *Int. Geol. Rev.* 53, 477-498, <https://doi.org/10.1080/00206814.2010.533873>
- Gulson, B.L., 1986. *Lead Isotopes in Mineral Exploration*. Elsevier Science Publishers, Amsterdam, 245p.
- Hall, D.L., Sterner, S.M., 1988. Freezing point depression of NaCl–KCl–H<sub>2</sub>O solution; *Econ. Geol.* 83, 197-202, <https://doi.org/10.2113/gsecongeo.83.1.197>
- Hessami, K., Jamali, F., Tabassi, H., 2003. *Major active faults of Iran*; International institute of earthquake engineering and seismology of Iran Press.
- Hitzman, M.W., Reynolds, N.A., Sangster, D.F., Allen, C.R., Carman, C.E., 2003. Classification, genesis, and exploration guides for nonsulfide zinc deposits. *Econ. Geol.* 98, 685-714. <https://doi.org/10.2113/gsecongeo.98.4.685>
- Hoefs, J., 1988. *Stable isotope geochemistry*. 3rd Ed. Berlin: Springer-Verlag. 241p.
- Huizenga, J.M., Gütmez, J., Banks, D., 2006. The Paleoproterozoic carbonate-hosted Pering Zn-Pb deposit, South Africa. II: fluid inclusion, fluid chemistry and stable isotope constraints; *Miner. Depos.* 40, 686-706. <http://doi.org/10.1007/s00126-005-0015-9>
- Jazi, M.A., Karimpour, M.H., Malekzadeh Shafaroudi, A., 2017. Nakhlak carbonate-hosted Pb-(Ag) deposit, Isfahan province, Iran: a geological, mineralogical, geochemical, fluid inclusion, and sulfur isotope study, *Ore Geo. Rev.* 80, 27-47, <https://doi.org/10.1016/j.oregeorev.2016.06.010>
- Jung, D., Keller, J., Khorasani, R., Marcks, Chr., Baumann, A., Horn, P., 1983. Petrology of the Tertiary magmatic activity the northern Lut area, East of Iran, Ministry mines and metals. Geological Survey of Iran, Geodynamic Project (Geotraverse) in Iran 51, 285-336.
- Karimpour, M.H., 2005. Comparison of Qaleh Zari Cu-Au-Ag deposit with other Iron Oxides Cu- Au (IOCG-Type) deposits and new classification. *Iranian J. Crystal. Mineral.* 13, 165-184.



Karimpour, M.H., Stern, C.R., 2009. Advance spaceborne thermal emission and reflection radiometer (ASTER) mineral mapping to discriminate high sulfidation, reduced intrusion related, and iron oxide gold deposits, eastern Iran. *J. Appl. Sci.* 9, 815-825, <http://doi.org/10.3923/jas.2009.815.828>

Karimpour, M.H., Stern, C.R., Farmer, L., Saadat, S., Malekzadeh Shafaroudi, A., 2011. Review of age, Rb-Sr geochemistry and petrogenesis of Jurassic to Quaternary igneous rocks in Lut Block, Eastern Iran. *Iranian Journal of Geopersia* 1(1) 19-36.

Karimpour, M.H., Malekzadeh Shafaroudi, A., Stern, C.R., Farmer, L., 2012. Petrogenesis of Granitoids, U-Pb zircon geochronology, Sr-Nd isotopic characteristic, and important occurrence of Tertiary mineralization within the Lut Block, eastern Iran. *Iranian J. Econ. Geol.* 41-27 (in Persian with English abstract).

Karimzadeh, A., 1992. Investigation on type, mineralogical-geochemical relationships, and the possible genesis of Emarat lead-zinc mine (Arak); M. Sc. Thesis, Tarbyat Moallem University, Tehran, Iran (In Farsi).

Kesler, S.E., 2005. Ore-forming fluids: *Elements* 1, 13-18, [https://doi:10.2113/gselements.1.1.13](https://doi.org/10.2113/gselements.1.1.13).

Lancelot, J., Orgeval, J., Fariss, K., Zadeh, H., 1997. Lead isotope signature of major Iranian Zn-Pb ore deposits (Anguran, Duna, Irankuh, Mahdiabad, Nakhlak). *Terra Nova (Abstract Supplement)* 1, 550.

Li, Y., Liu, J., 2006. Calculation of sulfur isotope fractionation in sulfides. *Geochim. Cosmochim. Acta* 70, 1789-1795. <http://doi.org/10.1016/j.gca.2005.12.015>.

Lotfi, M., 1982. Geological and Geochemical Investigation on the Volcanogenic Cu-Pb-Zn-Sb Ore Mineralization in the Shurab-Gale Chah and North West of Khur. Unpublished PhD Thesis, University of Hamburg, Hamburg, 1-152.

Lu, Z.C., Duan, G.Z., Liu, C.Q., Hao, L.B., Li, D.C., Wei, C.D., 2000. Daxing'anling Ag deposit types, metallogenic series and metallogenic geochemical characteristics. *Bull. Mineral. Petrol. and Geochem.* 19, 305-309 (in Chinese with English abstract).

Mahdavi, A., Karimpour, M.H., Mao, J., Haidarian Shahri, M.R., Li, H., 2016. Zircon U-Pb geochronology, Hf isotopes and geochemistry of intrusive rocks in the Gazu copper deposit. *Ore geol. Rev.* 72(1), 818-837, <https://doi.org/10.1016/j.oregeorev.2015.09.011>

Mahmoudi, S., Masoudi, F., Corfu, F., Mehrabi, B., 2010. Magmatic and metamorphic history of the Deh-Salm metamorphic Complex, Eastern Lut Block, (Eastern Iran), from U-Pb geochronology. *Int. J. Earth Sci.* 99, 1153-1165, <https://doi.org/10.1007/s00531-009-0465-x>

Malekzadeh Shafaroudi, A., 2009. Geology, Mineralization, Alteration, Geochemistry, Microthermometry, Radiogenic Isotopes, Petrogenesis of Intrusive Rocks and Determination of Source of Mineralization in Maherabad and Khopik Deposit, South Khorasan Province. Unpublished PhD Thesis, Ferdowsi University of Mashhad, Mashhad, Iran. 536p.

Malekzadeh Shafaroudi, A., Karimpour, M.H., Stern, C.R., 2012. Zircon U-Pb dating of Maherabad porphyry copper- gold deposit: evidence for a late Eocene porphyry-related metallogenic epoch in east of Iran. *Iranian Journal of Econ. Geol.* 3, 41-60. (In Persian with English abstract).

Malekzadeh Shafaroudi, A., Karimpour, M.H., 2013a. Hydrothermal alteration mapping in northern Khur, Iran, using ASTER image processing: a new insight to the type of copper mineralization in the area. *Acta Geol. Sin.* 87, 830-842. <http://doi.org/10.1111/1755-6724.12092>

Malekzadeh Shafaroudi, A., Karimpour, M.H., 2013b. Geology, mineralization, and fluid inclusion studies of the Howz-e-Rais lead-zinc-copper deposit, Eastern Iran. *Iranian J. Adv. Appl. Geol.* 6, 63-73 (in Persian with English abstract).

Malekzadeh Shafaroudi, A., Karimpour, M.H., 2015. Mineralogic, fluid inclusion, and sulfur isotope evidence for the genesis of Sechangi lead-zinc (-copper) deposit, Eastern Iran. *J. Afr. Earth Sci.* 107, 1-14, <https://doi.org/10.1016/j.jafrearsci.2015.03.015>

Malekzadeh Shafaroudi, A., Karimpour, M.H., Stern, C.R., 2015. The Khopik porphyry copper-gold prospect, Lut Block, Eastern Iran: geology, alteration, mineralization, fluid inclusion, and

oxygen isotope studies. *Ore geol. Rev.* 65(2), 522-544, <http://dx.doi.org/10.1016/j.oregeorev.2014.04.015>

Mehrabi, B., Talefazel, E., 2011. The role of magmatic and meteoric water mixing in mineralization of Shurab polymetal ore deposit, South of Ferdows: isotope geochemistry and microthermometry evidences. *Iranian J. Crystal. Mineral.* 19, 121-130 (in Persian with English abstract).

Mehrabi, B., Talefazel, E., Nokhbatolfoghahai, A., 2011. Disseminated, veinlet, and vein Pb–Zn, Cu and Sb polymetallic mineralization in the GaleChah-Shurab mining district, Iranian East Magmatic Assemblage (IEMA). *Iranian J. Econ. Geol.* 3, 61-77 (in Persian with English abstract).

Mirnejad, H., Simonetti, A., Molasalehi, F., 2011. Pb isotopic compositions of some Zn–Pb deposits and occurrences from Urumieh–Dokhtar and Sanandaj–Sirjan zones in Iran. *Ore Geol. Rev.* 39, 181-187, <https://doi.org/10.1016/j.oregeorev.2011.02.002>

Mirnejad, H., Simonetti, A., Molasalehi, F., 2015. Origin and formational history of some Pb-Zn deposits from Alborz and Central Iran: Pb isotope constraints. *Int. Geol. Rev.* 57(4), 463-471, <https://doi.org/10.1080/00206814.2015.1013510>

Mirzaei Rayeni, R., Ahmadi, A., Mirnejad, H., 2012. Mineralogy and fluid inclusion studies in Mahour polymetal deposit, east of Lut block, Central Iran. *Iranian J. Crystal. Mineral.* 20, 307-318 (in Persian with English abstract).

Moghadam, H.S., Stern, R.J., Rahgoshay, M., 2010. The Dehshir ophiolite (central Iran): geochemical constraints on the origin and evolution of the Inner Zagros ophiolite belt. *Geol. Soc. Am. Bull.* 122, 1516-1547, <http://doi.org/10.1130/B30066.1>

Mohajjel, M., Fergusson, C.L., Sahandi, M.R., 2003. Cretaceous–Tertiary convergence and continental collision, Sanandaj–Sirjan Zone, western Iran. *J. Asian Earth Sci.* 21, 397-412. [https://doi.org/10.1016/S1367-9120\(02\)00035-4](https://doi.org/10.1016/S1367-9120(02)00035-4)

Momenzadeh, M., Rastad, E., 1973. Zinc, lead and iron mineralization in Cretaceous crarbonatic rocks in the West-Central Iran metallogenic zone. *Geological Survey of Iran* 4 (In Farsi).

- Momenzadeh, M., 1976. Stratabound lead–zinc ores in the Lower Cretaceous and Jurassic sediments in the Malayer-Esfahan district (west central Iran), lithology, metal content, zonation and genesis. Ph.D. Thesis, Heidelberg University.
- Mousivand, F., Rastad, E., Meffre, S., Peter, J.M., Solomon, M., Zaw, K., 2011. U-Pb geochronology and Pb isotope characteristics of the Chahgaz volcanogenic massive sulphide deposit, southern Iran. *Int. Geol. Rev.* 53, 1239-1262, <https://doi.org/10.1080/00206811003783364>
- Ohmoto, H., 1972. Systematics of the sulfur and carbon in hydrothermal ore deposits. *Econ. Geol.* 67, 551-579, <https://doi.org/10.2113/gsecongeo.67.5.551>
- Ohmoto, H., Goldhaber, M.B., 1997. Sulfur and carbon isotopes. In: Barnes, H.L. (Ed.), *Geochemistry of Hydrothermal ore Deposits*. John Wiley and Sons, New York, pp. 517-611.
- Ohmoto, H., Rye, R.O., 1979. Isotopes of sulfur and carbon. In: Barnes, H.L. (Ed.), *Geochemistry of Hydrothermal ore Deposits*. Wiley, New York, pp. 509-567.
- Pang, K.N., Chung, S.L., Zarrinkoub, M.H., Khatib, M.M., Mohammadi, S.S., Chiu, H.Y., Chu Cn, H., Lee, H.Y., Lo, C.H., 2013. Eocene-Oligocene post-collisional magmatism in the Lut-Sistan region, eastern Iran: Magma genesis and tectonic implications, *Lithos*, 234-251, <https://doi.org/10.1016/j.lithos.2013.05.009>
- Pourabdollahi, A.R., 2009. Mineralogy and geochemistry of Chahsorb deposit, North of Tabas [M.Sc. thesis]. Shahid Beheshti University, 187 p.
- Rahimpour-Bonab, H., 1991. Investigation on lead-zinc deposits of South of Arak region (Emarat). M. Sc. Thesis. University of Tehran, Tehran, Iran (In Farsi).
- Ramboz, C., Pichavant, M., Weisbrod, A., 1982. Fluid immiscibility in natural processes: Use and misuse of fluid inclusion data. II. Interpretation of fluid inclusion data in terms of immiscibility. *Chem. Geol.* 37, 29-48, [https://doi.org/10.1016/0009-2541\(82\)90065-1](https://doi.org/10.1016/0009-2541(82)90065-1)

Ramezani, J., Tucker, R., 2003. The Saghand region, Central Iran: U–Pb geochronology, petrogenesis and implications for Gondwana tectonics. *Amer. J. Sci.* 303, 622-665, <https://doi.org/10.2475/ajs.303.7.622>

Reichert, J., 2007. A metallogenic model for carbonate-hosted non-sulfide zinc deposits based on observation of Mehdiabad and Irankuh, Central and Southwestern Iran [Ph.D. thesis]. Halle, Martin Luther University, Halle Wittenberg, 279 p.

Richards, J.P., Spell, T., Rameh, E., Razique, A., Fletcher, T., 2012. High Sr/Y magmas reflect arc maturity, high magmatic water content, and porphyry Cu±Mo±Au potential: examples from the Tethyan arcs of Central and Eastern Iran and Western Pakistan. *Econ. Geol.* 107, 295-332.

Robb, L., 2004. Hydrothermal processes. In: Robb, L. (Ed.), *Introduction to Ore forming Processes*. Wiley, New York, pp. 127-215, <https://doi.org/10.2113/econgeo.107.2.295>

Robertson, A.H.F., 2007. Overview of tectonic settings related to the rifting and opening of Mesozoic ocean basins in the Eastern Tethys: Oman, Himalayas and Eastern Mediterranean regions. In: Karner, G., Manatschal, G., Pinheiro, L. (Eds.), *Imaging, Mapping and Modelling of Continental Lithosphere Breakup*. Geological Society London Special Publication 282, 325-388.

Roedder, E., 1958. Technique for the extraction and partial chemical analysis of fluid-filled inclusions from minerals. *Econ. Geol.* 53, 235-269, <https://doi.org/10.2113/gsecongeo.53.3.235>

Roedder, E., 1972. The composition of fluid inclusions. *US Geological Survey Professional Paper*, 164 p.

Roedder, E., 1984. *Fluid Inclusions; Reviews in Mineralogy*. Mineralogical Society of America, Washington, DC 12, 1-644.

Routner, A., Nabavi, M.H., Alavi Naieni, M., 1994. Geological map of Eshgh-Abad, Scale 1:100000, Geological Survey of Iran.

Saccani, E., Delavari, M., Beccaluva, L., Amini, S.A., 2010. Petrological and geochemical constraints on the origin of the Nehbandan ophiolitic complex (eastern Iran): implication for the evolution of the Sistan Ocean. *Lithos* 117, 209-228, <https://doi.org/10.1016/j.lithos.2010.02.016>

- Sadeghibojd, M., 1995. Origin of lead mineralization in Shotori formation, Tabas area, Khorasan province [M.Sc. thesis]. University of Shiraz, 267 p.
- Samani, B.A., 1988. Metallogeny of the Precambrian in Iran. *Precambr. Res.* 3, 85-106, [https://doi.org/10.1016/0301-9268\(88\)90053-8](https://doi.org/10.1016/0301-9268(88)90053-8)
- Samani, B., Ashtari, S., 1992. Geological evolution of Sistan and Baluchestan area. *Iranian J. Geosci.* 4, 72–85 (in Persian with English abstract).
- Sengör, A.M.C., 1990. A new model for the late Paleozoic–Mesozoic tectonic evolution of Iran and implications for Oman. In: Robertson, A.H.F., Searle, M.P., Ries, A.C. (Eds.), *The Geology and Tectonics of the Oman Region*. Geological Society London Special Publication 49, 797-831.
- Shepherd, T.J., Rankin, A.H., Alderton, D.H.M., 1985. *A Practical Guide to Fluid Inclusion Studies*. Blackie, London, UK.
- Shojaat, B., 1992. Geochemical investigations in order to propose possible model for lead-zinc mineralization in the Emarat region. M. Sc. Thesis, Islamic Azad University, North Tehran Branch, Iran (In Farsi).
- Stacey, J.S., Kramers, J.D., 1975. Approximation of terrestrial lead isotope evolution by a two-stage model. *Earth Planet. Sci. Lett.* 26, 207-221, [https://doi.org/10.1016/0012-821X\(75\)90088-6](https://doi.org/10.1016/0012-821X(75)90088-6)
- Stampfli, G.M., Borel, G.D., 2002. A plate tectonic model for the Paleozoic and Mesozoic constrained by dynamic plate boundaries and restored synthetic oceanic isochrones. *Earth Planet. Sci. Lett.* 196, 17-33, [https://doi.org/10.1016/S0012-821X\(01\)00588-X](https://doi.org/10.1016/S0012-821X(01)00588-X)
- Stöcklin, J., 1968. Structural history and tectonics of Iran; a review. *AAPG Bull.* 52, 1229-1258.
- Stöcklin, J., Nabavi, M.H., 1969. Geological map of Boshrouyeh, Scale 1:250000, Geological Survey of Iran.
- Stöcklin, J., Eftekhamejad, J., Hoshmandzadeh, A., 1971. Initial investigation of central Lut block, eastern Iran. Geological Survey of Iran, 88 p.
- Stöcklin, J., Nabavi, M.H., 1973. Tectonic map of Iran. Geological Survey of Iran.

- Stöcklin, J., 1974. Possible ancient continental margins in Iran. In: Burk, C.A., Drake, C.L. (Eds.), *The Geology of Continental Margins*. Springer, Berlin 873-887.
- Sverjensky, D.A., 1987. Genesis of Mississippi Valley-type lead–zinc deposits. *Annu. Rev. Earth Planet. Sci. Letters* 14, 177-199, <https://doi.org/10.1146/annurev.ea.14.050186.001141>
- Takin, M., 1972. Iranian geology and continental drift in the Middle East. *Nat. Geosci.* 235, 147-150.
- Tarkian, M., Lotfi, M., Baumann, A., 1982. Tectonic, magmatism and the formation of mineral deposits in the central Lut, east Iran. Ministry of mines and metals, Geological Survey of Iran, geodynamic Project in Iran 51, 357-383.
- Tirrul, R., Bell, I.R., Griffis, R.J., Camp, V.E., 1983. The Sistan suture zone of eastern Iran. *Geol. Soc. Amer. Bull.* 94, 134-156, [https://doi.org/10.1130/0016-7606\(1983\)94<134:TSSZOE>2.0.CO;2](https://doi.org/10.1130/0016-7606(1983)94<134:TSSZOE>2.0.CO;2)
- Van den Kerkhof, A.M., Hein, U., 2001. Fluid inclusion petrography. *Lithos* 55, 27-47, [https://doi.org/10.1016/S0024-4937\(00\)00037-2](https://doi.org/10.1016/S0024-4937(00)00037-2)
- Vanaei, M., 1998. Textural, structural and geochemical characteristics of Emarat Pb-Zn mine (Arak). M. Sc. Thesis, Shahid Bahonar University, Kerman, Iran (In Farsi).
- Walker, R., Jackson, J., 2004. Active tectonics and late Cenozoic strain distribution in central and eastern Iran. *Tectonics* 23, TC5010, <https://doi.org/10.1029/2003TC001529>
- Walker, R.T., Gans, P., Allen, M.B., Jackson, J., Khatib, M., Marsh, N., Zarrinkoub, M., 2009. Late Cenozoic volcanism and rates of active faulting in eastern Iran. *Int. J. Geophys.* 177, 783-805, <https://doi.org/10.1111/j.1365-246X.2008.04024.x>
- Whitney, D.L., Evans, B.W., 2010. Abbreviations for names of rock-forming minerals. *Amer. Miner.* 95, 185-187, <https://doi.org/10.2138/am.2010.3371>
- Wilkinson, J.J., 2001. Fluid inclusions in hydrothermal ore deposits. *Lithos* 55 (1-4), 229-272, [https://doi.org/10.1016/S0024-4937\(00\)00047-5](https://doi.org/10.1016/S0024-4937(00)00047-5)

- Zanchi, A., Zanchetta, S., Berra, F., Mattei, M., Garzanti, E., Molyneux, S., Nawab, A., Sabouri, J., 2009. The Eo- Cimmerian (Late? Triassic) orogeny in North Iran. Geological Society, London, Special Publications 312, 31-55. <https://doi.org/10.1144/SP312.3>.
- Zarrinkoub, M.H., Pang, K.N., Chung, S.L., Khatib, M.M., Mohammadi, S.S., Chiu, H.Y., Lee, H.Y., 2012. Zircon U-Pb age and geochemical constraints on the origin of the Birjand ophiolite, Sistan suture zone, eastern Iran. *Lithos* 154, 392-405, <https://doi.org/10.1016/j.lithos.2012.08.007>
- Zartman, R.E., Doe B.R., 1981. Plumbotectonics – the model. *Tectonophysics* 75, 135-162, [https://doi.org/10.1016/0040-1951\(81\)90213-4](https://doi.org/10.1016/0040-1951(81)90213-4)
- Zartman, R.E., Haines, S.M., 1988. The plumbotectonic model for Pb isotopic systematics among major terrestrial reservoirs – a case for bidirectional transport. *Geochim. Cosmochim. Acta* 52, 1327-1339, [https://doi.org/10.1016/0016-7037\(88\)90204-9](https://doi.org/10.1016/0016-7037(88)90204-9)
- Zhai, D.G., Liu, J.J., Wang, J.P., Yao, M.J., Wu, S.H., Fu, C., Liu, Z.J., Wang, S.G., Li, Y.X., 2013. Fluid evolution of the Jiawula Ag–Pb–Zn deposit, Inner Mongolia: mineralogical, fluid inclusion, and stable isotopic evidence. *Int. Geol. Rev.* 55, 204-224, <https://doi.org/10.1080/00206814.2012.692905>
- Zhang, D.H., 1997. Some new advances in ore forming fluid geochemistry on boiling and mixing of fluids during the processes of hydrothermal deposits. *Ad. Earth Sci.* 12, 546-550 (in Chinese with English abstract). <https://doi.org/10.1080/00206810109465026>
- Zhu, Y.F., Zeng, Y.S., Jiang, N., 2001. Geochemistry of the ore-forming fluids in gold deposits from the Taihang Mountains, northern China. *Int. Geol. Rev.* 43, 457-473, Ziserman, A., Momenzadeh, M., 1972. Study on Arak-Esfahan lead-zinc mine. Geological Survey of Iran 60, 16 p. (In Farsi).



**Highlights**

- The Kaviro lead vein deposit in the Lut Block is emplaced in folds.
- Ore-forming fluids are of medium-to-low temperature.
- Sulfur isotopes suggest a nonmagmatic source for the ore-forming aqueous solutions.
- The Pb isotopic results show a continental crust source for Pb.
- Metamorphic fluids are responsible for the mineralization in the Kaviro deposit.

ACCEPTED MANUSCRIPT